DESIGN AND CONSTRUCTION OF BOUNDARY LUBRICATED BEARING TEST RIG AND WEAR ANALYSIS IN EARTHMOVING MACHINERY

A THESIS SUBMITTED TO
THE GRADUATE SCHOOL OF NATURAL AND APPLIED SCIENCES
OF
MIDDLE EAST TECHNICAL UNIVERSITY

BY

KORAY SERDAR TEKİN

IN PARTIAL FULFILLMENT OF THE REQUIREMENTS
FOR
THE DEGREE OF MASTER OF SCIENCE
IN
MECHANICAL ENGINEERING

DECEMBER 2010

Approval of the thesis:

DESIGN AND CONSTRUCTION OF BOUNDARY LUBRICATED BEARING TEST RIG AND WEAR ANALYSIS IN EARTHMOVING MACHINERY

submitted by **KORAY SERDAR TEKİN** in partial fulfillment of the requirements for the degree of **Master of Science in Mechanical Engineering Department, Middle East Technical University** by,

Prof. Dr. Canan Özgen _____
Dean, Graduate School of **Natural and Applied Sciences**

Prof. Dr. Suha Oral _____
Head of Department, **Mechanical Engineering**

Prof. Dr. Metin Akkök _____
Supervisor, **Mechanical Engineering Dept., METU**

Prof. Dr. Eres Söylemez _____
Co-Supervisor, **Mechanical Engineering Dept., METU**

Examining Committee Members:

Prof. Dr. Suat KADIOĞLU _____
Mechanical Engineering Dept., METU

Prof. Dr. Metin AKKÖK _____
Mechanical Engineering Dept., METU

Prof. Dr. Eres SÖYLEMEZ _____
Mechanical Engineering Dept., METU

Asst. Prof. Ender CİĞEROĞLU _____
Mechanical Engineering Dept., METU

Ferhan Fıçıcı, M.Sc. _____
Team Leader of R&D, Hidromek Inc.

Date: _____

I hereby declare that all information in this document has been obtained and presented in accordance with academic rules and ethical conduct. I also declare that, as required by these rules and conduct, I have fully cited and referenced all material and results that are not original to this work.

Name, Last name : Koray Serdar TEKİN

Signature :

ABSTRACT

DESIGN AND CONSTRUCTION OF BOUNDARY LUBRICATED BEARING TEST RIG AND WEAR ANALYSIS IN EARTHMOVING MACHINERY

Tekin, Koray Serdar
M.Sc., Department of Mechanical Engineering
Supervisor : Prof. Dr. Metin Akkök
Co-Supervisor : Prof. Dr. Eres Söylemez

December 2010, 94 pages

Excavators which used as earthmoving machinery are exposed to heavy loads and operate long hours repeatedly. The forces that are transmitted trough pin bearings are observed to cause failure due to wear. Therefore, durability of bearings is crucial for excavators. The aim of this study is to perform wear analysis of excavator bearings running in boundary lubrication regime. A hydraulically powered test rig, which simulates the operating conditions of excavator bearings is designed and constructed. Wear is obtained applying both force and relative motion between pin and bearing on the test rig. Several tests are performed in this test bench. Force and material type are varied as the factors influencing wear. Results are compared and the effects of the factors on wear are determined.

Keywords: Wear Test, Excavator, Bearing, Boundary Lubrication

ÖZ

SINIR YAĞLAMA KOŞULLARINDA ÇALIŞAN KAYMALI YATAKLAR İÇİN TEST DÜZENEĞİ TASARIMI, YAPIMI VE İŞ MAKİNELERİNDE AŞINMA ANALİZİ

Tekin, Koray Serdar
Yüksek Lisans, Makina Mühendisliği Bölümü
Tez Yöneticisi : Prof. Dr. Metin Akkök
Ortak Tez Yöneticisi : Prof. Dr. Eres Söylemez

Aralık 2010, 94 sayfa

Ekskavatörler yüksek yüklemelere maruz kalan ve uzun saatler boyunca çalışan iş makineleridir. Pim ve yataklar aracılığıyla iletilen kuvvetlerin aşınmaya sebep olduğu görülmüştür. Bu çalışmanın amacı sınır yağlama koşullarında çalışan ekskavatör yataklarının aşınma analizinin yapılmasıdır. Ekskavatör yataklarının çalışma koşullarının simüle edilebildiği hidrolik tahrikli bir deney düzeneği tasarlanıp üretilmiştir. Aşınma, pim ve yatak arasında kuvvet ve hareketin aynı anda sağlanmasıyla elde edilmiştir. Çeşitli testler yapılmıştır. Aşınmayı etkileyen, hız, kuvvet, materyal tipi gibi özellikler değişimli denenmiştir. Sonuçlar karşılaştırılıp bu faktörlerin aşınma üzerindeki etkileri bulunmuştur.

Anahtar kelimeler: Aşınma Testi, Ekskavatör, Kaymalı Yatak, Sınır Yağlama

God made the solids, but surfaces were the work of the devil.

Wolfgang Pauli
Physicist

ACKNOWLEDGMENTS

I wish to express my deepest gratitude to my supervisor Prof. Dr. Metin AKKÖK for his guidance, advice, criticism, encouragements and insight throughout the research.

I would like to state my sincere thanks to my co-supervisor Prof. Dr. Eres SÖYLEMEZ for his guidance, motivation, supervision and patience.

I would like to thank my colleagues Ferhan FIÇICI, Cevdet Can UZER, Tarık OLĞAR, Erkal ÖZBAYRAMOĞLU, Boran KILIÇ, Tuğçe YALÇIN and Durmuş Ali GÖZTAŞ for their suggestions and comments; Eşref YÜRÜKLÜ and İrfan BOSTANLI for their help.

I would also like to express my appreciation to Hasan Basri BOZKURT, general manager of Hidromek Inc., for his support.

Finally, I would like to express my thanks to my parents for their support and continuous faith in me.

This study is supported by Hidromek Inc.

TABLE OF CONTENTS

LIST OF TABLES

TABLES

LIST OF FIGURES

FIGURES

LIST OF SYMBOLS AND ABBREVIATIONS

SYMBOLS

h : Wear Depth

$\dot{h}$: Wear Rate

s : Sliding Distance

f^* : Uncertainty Factor

w : Width of the Bearing

A : Projected Area

A_r : Real Contact Area

D : Diameter of the Bearing

E : Young's Modulus

F : Force

H_{soft} : Hardness of the Softer Material

N : Angular Speed

N_f : Test Cut-Off Time

K : Wear Rate / Coefficient

P : Pressure

Q : Load per Unit Pin Length

R : Stress Ratio

R_1 : Pin Radius

R_2 : Bearing Radius

R_a : Arithmetic Average Surface Roughness

S_m : Modified Shear Strength

S^*_m : Modified Shear Strength at Scuffing Onset

V : Linear Velocity of the Bearing

V_{wear} : Wear Volume

ΔR : Radial Clearance

α : Contact Angle

β : Oscillating Angle in Degrees

μ : Coefficient of Friction

μ_d : Dynamic Viscosity

ν : Kinematic Viscosity

δ : Density

τ : Shear Stress

τ_m : Maximum Surface Tangential Traction

τ^*_m : Maximum Surface Tangential Traction at Scuffing Onset

σ : Force per Unit Projected Area

ABBREVIATIONS

AISI : American Iron and Stell Institute

CMM : Coordinate Measuring Machine

HRC : Rockwell Hardness in C-Scale

JIS : Japanese Industrial Standards

LVDT : Linear Variable Differential Transformer

PTFE : Polytetrafluoroethylene

PV : Pressure Velocity Multiplication

SEM : Scanning Electron Microscobe

CHAPTER 1

INTRODUCTION

Excavators are engineering vehicles, which are primarily used for the purpose of digging trenches, holes or foundations. These equipment are exposed to heavy loads and work long hours repeatedly. The digging forces are transmitted by bearings in excavator attachments. Hence, some failure problems are observed in excavator bearings. Generally, the failure type is wear, whereas sometimes fatigue cracks can be observed.

Excavators can be utilized in regions where service requirements may not be satisfied in short time periods. Therefore, durability of every part is crucial for excavators. High wear resistance is desired in excavator bearings.

This study aims to perform a wear analysis of excavator bearings and compare the wear behavior of bearings for different operating conditions.

1.1. Basic Construction of Excavators

Excavators are the mobile machines, which have an upper structure capable of continuous rotation and dig, elevate, swing and dump material [1]. These machines are utilized in heavy conditions, since large amount of bulk material is of concern. They are hydraulically operated in order to create high forces for the required job to be done.

Excavators consist of a boom, an arm and a bucket on a rotating upper chassis, as shown in Figure 1.1. The upper chassis sits on a platform with tracks or wheels, called lower chassis, on which it can fully rotate [1]. The boom – arm – bucket mechanism is a three-degree of freedom system that is controlled by hydraulic cylinders. In the working range of this mechanism, the bucket can be moved to any point and can perform digging operation.

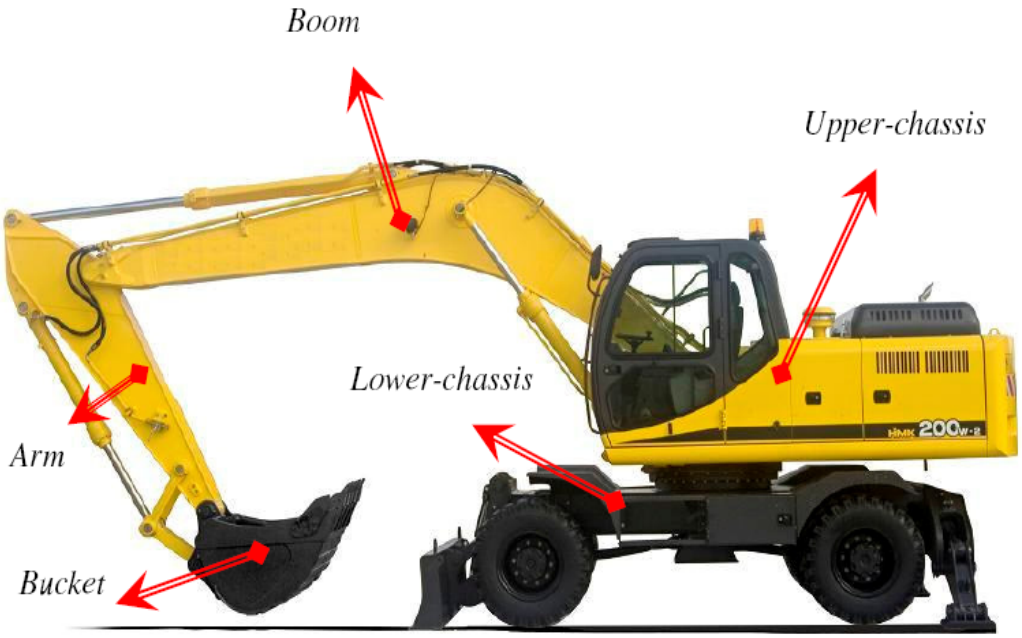

Figure 1.1 - General view of an excavator

By the help of a powerful diesel engine and hydraulic power utilization, excavators can dig, move and dump large amount of soil. The forces coming from soil and attachment weights are transmitted to the chassis through the joints of the attachments of the excavator. Therefore, large forces are created in the joints, which also changes direction while the mechanism is in use.

The hydraulic cylinders, used as the actuators of the mechanism, have prismatic joints. A rod can be moved freely in a cylinder in axial direction. Apart from the hydraulic cylinders, all joints of the boom – arm – bucket mechanism can be classified as revolute joints. Joining is performed by solid cylindrical pins on which bearings can rotate. The bearings are tightly fitted to the joint holes on attachments. A pin is placed through the bearings of both attachments, where the links of the mechanism are desired to be joined. The pin is also fixed to one of the links, so that it cannot rotate freely or come out, as can be seen in Figure 1.2.

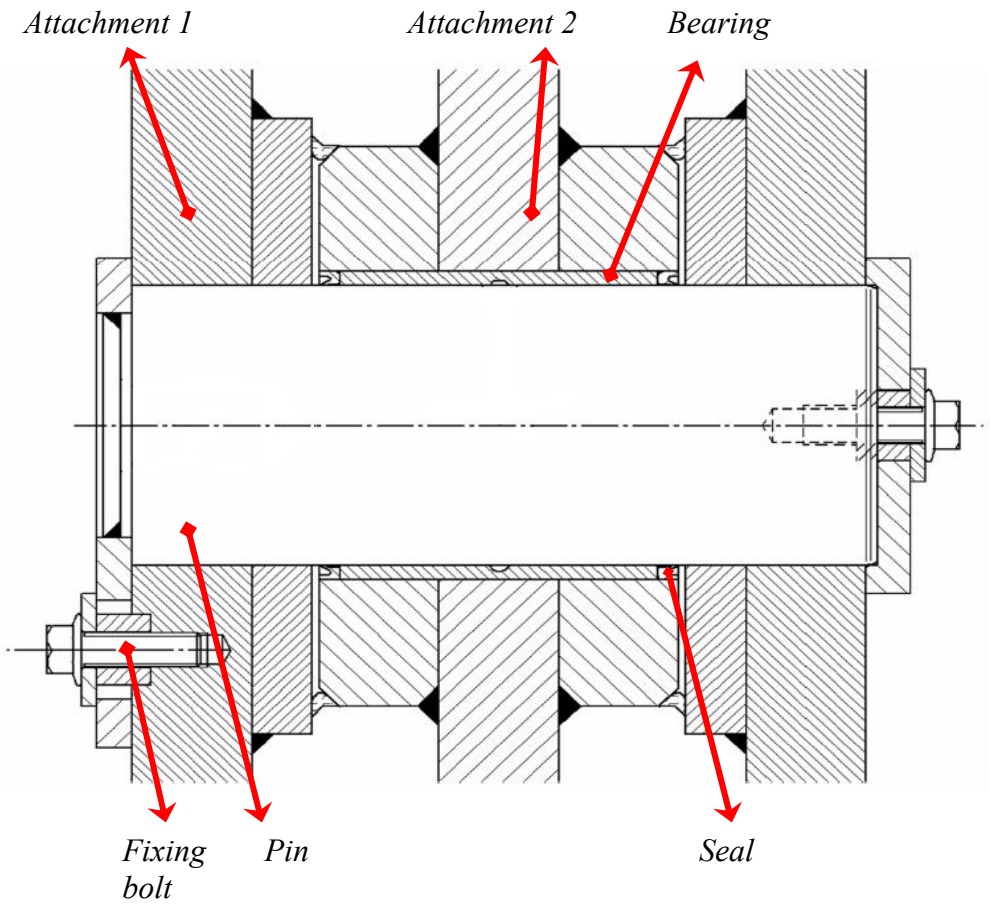

Figure 1.2 – Cross-section of a typical journal bearing mounting [2]

1.2. Bearing Load and Velocity Values during Operation of Excavators

Excavator bearings may be exposed to different load and velocity values, depending on the force at the bucket tip. The force and velocity at bearings are inversely proportional to each other, giving a constant engine power. Without load, the attachment movements, and therefore the bearing rotations, are fast; however, when the force is introduced to bucket tip, movements slow down.

In 22-ton excavators, when there is no load, the boom foot may be exposed up to 210 kN force values, stemming just from the attachment weights. Since the boom foot has two bearings, 105 kN force per bearing is observed. In this no-load case, the hydraulic system can maintain a rotational velocity of 15 - 20°/s at boom foot depending on mechanism position.

Bearings are generally loaded to their maximum value while digging. This load is limited by either hydraulic relief pressure or tipping of the excavator. In this case, one bearing at boom foot can be loaded up to 230 kN at 4 - 5°/s speed.

1.3. Bearing Lubrication and Wear

The force and velocity values given in Section 1.2 yield a result regarding the lubrication regime. Excavator boom foot bearings, or any other, are in boundary lubrication condition. This phenomenon can be described by the Stribeck curve. The hydrodynamic film thickness is proportional to the lubricant viscosity and sliding velocity, inversely proportional to the applied load. Shigley [4] recommends a bearing characteristic value for thick film lubrication:

$$\frac{\mu_d N}{P} > 1.7 \times 10^{-6} \tag{1.1}$$

Where μ_d is the dynamic viscosity of oil (Pa.s), N is angular speed (rps) and P is average bearing pressure (Pa). Finding the dynamic viscosity of the grease at 40°C, from the kinematic viscosity, ν, and density of grease, δ [5]:

$$\mu_d = \upsilon \text{ x } \delta \tag{1.2}$$

$$\mu_d = 1.8 \text{ x } 10^{-4} \text{ m}^2/\text{s x } 1000 \text{ kg/m}^3 \tag{1.3}$$

$$\mu_d = 0.18 \text{ Pa.s} \tag{1.4}$$

Pressure is calculated using the projected area of bearing, where the diameter of the boom foot bearing is 100 mm and bearing width is 110 mm:

$$P = \frac{F}{D \text{ x } w} \tag{1.5}$$

$$P = \frac{105000 \text{ N}}{100 \text{ mm x } 110 \text{ mm}} = 9.54 \text{ MPa} \tag{1.6}$$

When 0.044 rps, which is equivalent to 16 °/s, angular speed and 105 kN bearing load are used in equation (1.1):

$$\frac{\mu_d N}{P} = \frac{0.18 \text{ Pa. s x } 0.044 \text{ rps}}{9.54 \text{ x } 10^6 \text{ Pa}} \tag{1.7}$$

$$\frac{\mu_d N}{P} = 8.3 \text{ x } 10^{-10} \tag{1.8}$$

which shows that lubrication regime is boundary lubrication.

Wear is process of a loss of substance from a solid body surface in frictional conditions, which appears as a gradual decrease of body dimensions and/or change of

shape [3]. It is an undesirable situation, because with uncontrolled dimensional changes, a mechanical system may malfunction, or become totally useless. A common example is the seizure phenomenon. Seizure is the local welding of two mating components and stop of the relative motion between them. A view of seizure can be seen in Figure 1.3. Therefore, wear rate for mating surfaces should be as low as possible. Wear rate depends on controllable and measurable quantities such as relative velocity and pressure of mating surfaces, and operating time of mating pairs. However, it also depends on hardness and roughness values of mating surfaces, lubricant type, lubricant amount, temperature of mating surfaces and many other factors. These factors are usually uncontrolled and may change with time as mating surfaces work against each other.

Figure 1.3 - A View of seizure on a bearing

From this point forth, it is seen that, pins and bearings at the mechanism joints of excavator attachments are in contact because of the forces that are transmitted. Also, there is a relative motion between pin and bearing since linkages rotate with respect to each other. Therefore, wear is a common problem on pin-bearing couples at the joints of excavators. Material and surface characteristics of pin and bearing have to be chosen wisely in order to eliminate wear. Also, to minimize wear, grease is used as a lubricant third body between the mating surfaces of pins and bearings. As surfaces rub against each other, grease gets dirty by debris from metals or dust, therefore it is changed periodically.

1.4. Scope of the Thesis

The aim of this study is to construct a test bench for wear measurement of excavator bearings, analyze bearing wear with different test parameters and comparison with tests. Firstly, a test bench is designed and constructed. Boom foot bearing is selected for testing. To simulate the real forces on this bearing, hydraulic power is utilized and the load variation and speed are precisely controlled. Then, on the test bench, the bearings are exposed to oscillatory forces, similar to those on excavators. The tests are repeated with different forces and velocities for two different bearing types. The test results are analyzed and a suitable bearing is recommended for excavator joints.

The literature on bearing wear stemming from boundary lubrication will be given in the second chapter. The third chapter includes theoretical information about wear types. In the fourth chapter, the components and operating principles of the test bench are introduced. Fifth chapter is on the procedure of wear tests and profile measurements. Lastly, results and discussion are given in sixth chapter.

CHAPTER 2

LITERATURE SURVEY ON BEARING WEAR

Theoretical and experimental studies on bearing wear are given in this section. Experimental studies are in majority, since wear phenomenon is difficult to model and sensitive to environmental effects. Generally, comparison tests are performed for a particular situation to determine the optimum bearing properties.

2.1. Theoretical Studies on Bearing Wear

Kim et al. [6] studied the steel - steel oscillatory contact in finite element analysis. Firstly, oscillating pin-on-disc experiments were performed to determine the wear rate of steel – steel contact. The definition of wear rate in the study is volume loss per unit work, where work is time averaged pin force times sliding distance. The wear rate is found out as 1×10^{-5} mm^3/Nm from pin-on-disc experiments. Using this wear rate, a block-on-ring wear phenomenon is modeled and analyzed by a finite element tool, as can be seen in Figure 2.1. The outer diameter of the ring is 35 mm; the projected area of the block is 100 mm^2. The ring is oscillated ±3°. 470 N load is applied and 1098.8 m sliding distance is taken.

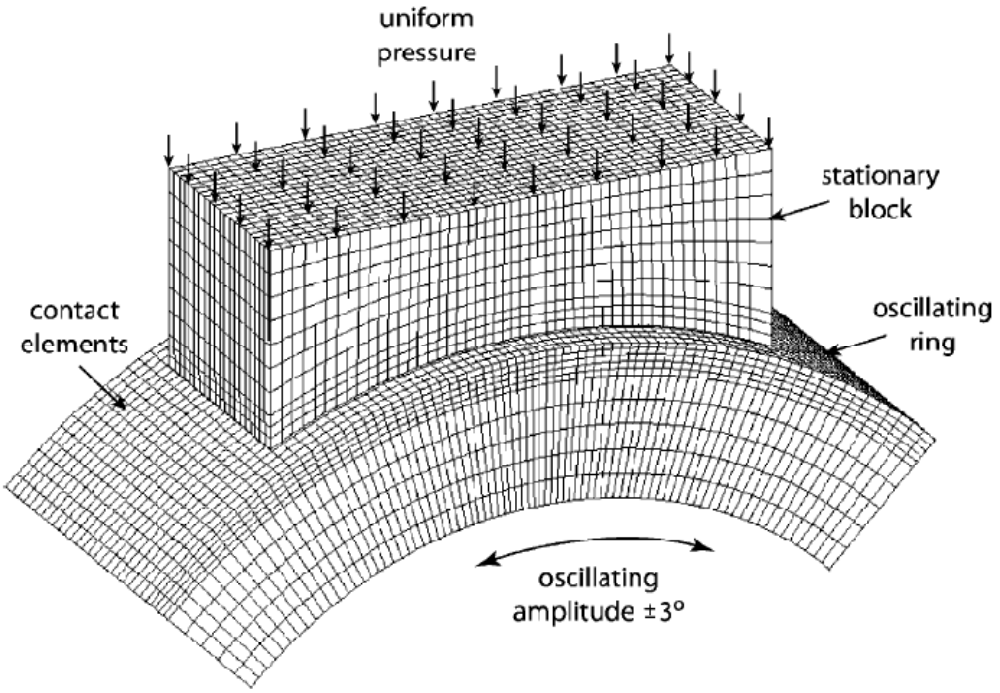

Figure 2.1 - Finite element model of the block-on-ring simulation [6]

For the confidence of study, experimental validation is needed. Two tests were performed with the same conditions as FEM analysis; where up to 88% agreement is observed. Results can be seen in Figure 2.2.

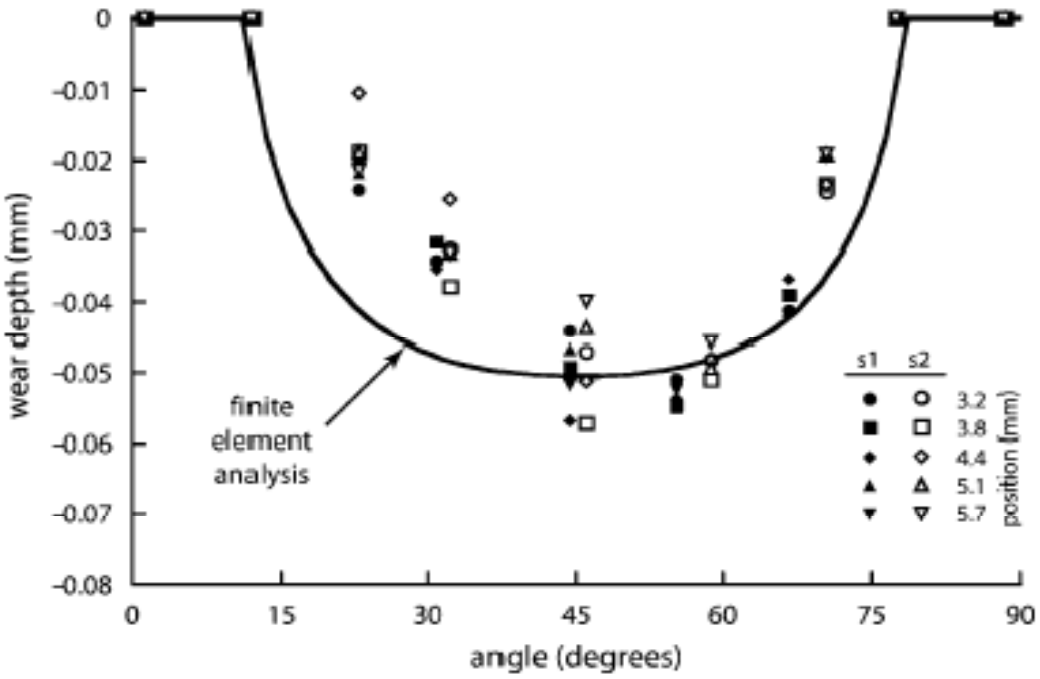

Figure 2.2 – Comparison of FEA and experiment results [6]

In a bearing assembly for construction equipment, geometry of the assembly has also an effect in bearing wear. An even pressure distribution in a bearing reduces contact pressure peaks, and prevents wear. This pressure distribution can be obtained by an optimum stiffness of housing and pin. Strand [2] made a statistical study on journal bearing housing design for optimum pressure distribution. FEM analyses of a pin-bearing-housing assembly are performed with different housing dimensions. The parameters are selected as set ring thickness, set ring width and weld size. The features are in Figure 2.3. 27 runs were performed, varying each parameter at three levels. The resulting pressure distributions are compared. The least squares fit and RMS deviation values of pressure distributions were compared. It was found out that the weld size has little influence on pressure distribution, 98% of influence is caused by the set ring width and thickness parameters. The best shape for a set ring came out to be circular. Also, set ring thickness should be kept low.

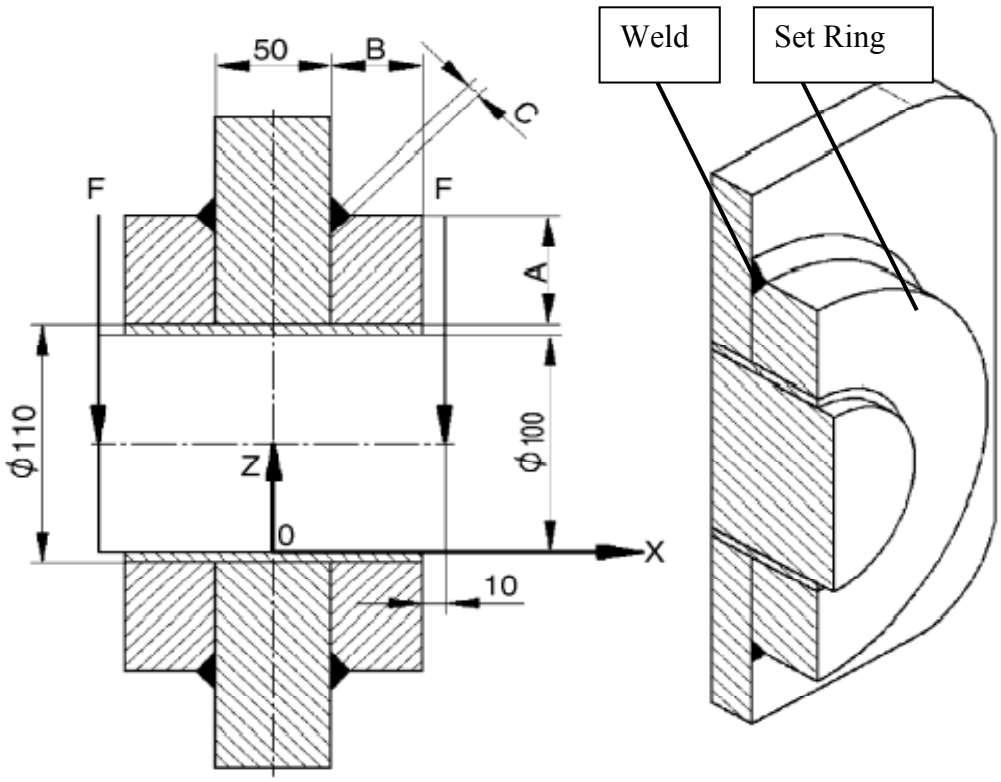

Figure 2.3 – Bearing mounting parameters [2]

Dickrell and Sawyer [7] constructed a 2-D wear model for a shaft-bearing system. They assumed a constant contact angle, a uniform pressure distribution and a non-cycle dependent wear rate between shaft and bearing. The progression of radial wear of shaft and bearing is evaluated. One outcome from the model is that the contact angle, α, is extremely dependent on ratio of wear rates of mating materials, as can be seen in Figure 2.4. K_s* stands for the ratio of shaft wear rate to bearing wear rate and K_b* is the reciprocal of K_s*. Also a test setup is prepared for checking the theory developed. A brass shaft - brass bearing and a brass shaft - PTFE bearing tests are performed. 650 N load is applied to the Φ19 mm shaft. The tests are performed with a 50.8 mm/s speed. The wear rate of PTFE came out to be transient, in other words, wear rate changes as the test continues. This behavior is thought to be questionable, since an ever-growing thin PTFE debris film on the shaft observed at the end of the

test. Also, it is stated that to have considerable wear on both components, the ratio of wear rates should be close.

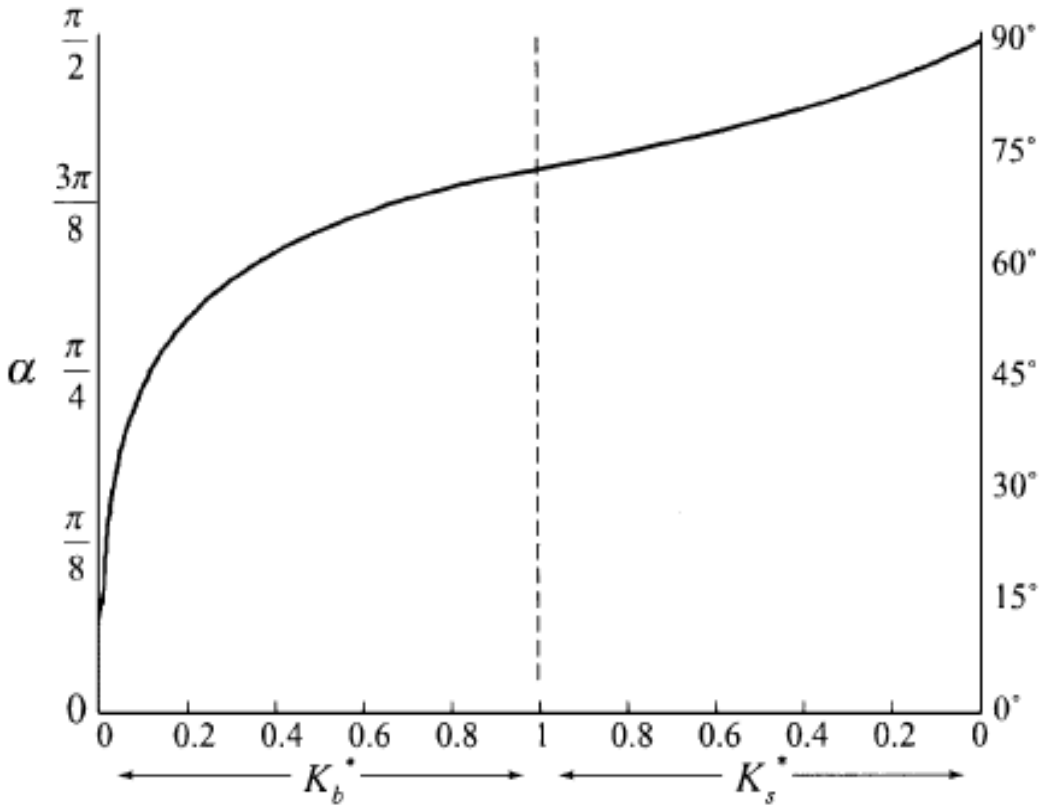

Figure 2.4 – Wear rate ratio vs contact angle [7]

2.2. Experimental Studies on Bearing Wear

In many cases, identification of wear type might be difficult, since different types might be observed at the same time. For instance, adhesive wear between two surfaces results in small broken particles, called debris, which are trapped between mating surfaces. Debris are harder than the base material because of strain hardening effect, so they cut the base material around. Therefore, adhesive and abrasive wear

may couple in such cases [8]. Also, wear is very sensitive to environmental conditions. Because of these facts, modeling and analytical evaluation of these phenomena is a difficult process and a limited agreement between analytical solution and validation tests can be obtained. Therefore, wear is studied generally based on experiments.

While scientific investigators study the fundamentals of material properties by standardized tests such as pin-on-disc test; every industry needs to reproduce its particular conditions, leading much focused test procedures and equipment [8]. All tests, in common, tries to simulate the real application as well as possible. Different parameters are varied and a comparison or correlation is set up.

Ukonsaari et al. [9], set up a test rig that simulates the rotor bearing of a Kaplan water turbine. The aim is to perform controlled experiments and compare friction and wear results of systems with different synthetic ester lubricants. The tests were performed with a steel shaft and a bronze bearing, whose alloy contents are known. The motion here is simulated to be a slow intermittent motion and the lubrication regime is boundary lubrication, which is the case in Kaplan turbines. Φ40 mm diameter and 32 mm length bearings were used. 5000 m sliding distance is taken by 10.5 mm/s sliding speed with ±60° oscillations. Three lubricant types, A, B and C, were investigated. A is a pure modified polyol ester. B and C are the different formulations of base fluid containing different anti-wear additives. All the lubricants are tested under two different pressure values, 30 MPa and 50 MPa. The wear coefficients, K, were calculated by using the wear volume, V_w, load applied, F, and sliding distance, s, with equation (2.1).

$$K = \frac{V_{wear}}{F.s} \tag{2.1}$$

The wear rate came out to be load dependent in one lubricant type, whereas the other lubricants gave similar wear rate results in different loads, as can be seen in Figure

2.5. Also to investigate micro scale damage, SEM/EDS mapping is done. The steel-bronze contact switched to copper-steel or copper-copper contact, since copper layer formation on steel shaft is observed. This layer formation was stated to be an advantage.

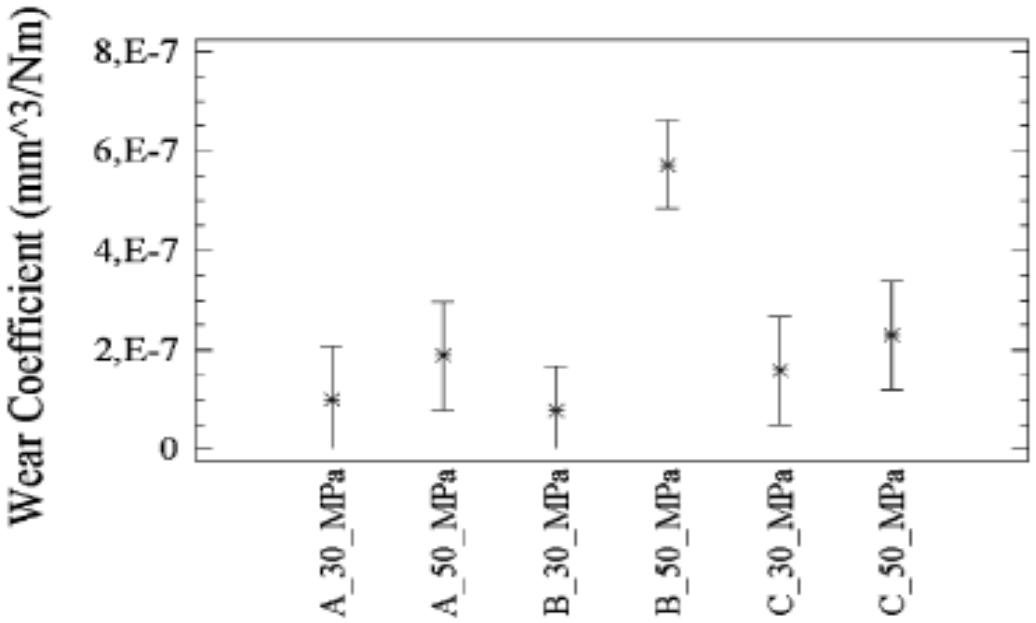

Figure 2.5 – Wear coefficients for lubricants A, B, C under 30 and 50 MPa bearing pressure [9]

Andersson et al. [10] studied the running-in behavior of water lubricated SiC journal bearings. They claim that the wear in start-up events is in considerable amount compared to the normal running period. Because, sleeve and bearing are exposed to wear in boundary and mixed conditions. Different sintered silicon carbides (SiC), silicon infiltrated silicon carbide (SiSiC) and graphite added SiSiC (C-SiSiC) are chosen as test materials. For wear determination, weight loss, stylus measurement and SEM visioning are performed. SiC materials are observed to give a little amount

of wear in boundary and fluid film regimes. Both the sleeve and bearing surfaces are polished, causing an increase on permissible on pressure on the real area of contact. Wear of SiSiC material is higher than that of SiC material due to the tendency of silicon phase to tribochemical wear in water. Although the mechanical properties of C-SiSiC material are not as good as SiC material, owing to the internal lubricating graphite phase, its wear remained low.

Khonsari and Lu [11] studied the effect of dimples on frictional behavior of journal bearings. Dimples are the potholes on inner surface of bearings in which the lubricant is stored, as can be seen in Figure 2.6. They performed comparative experiments where load, oil type, dimple size and shape, are varied. Both the mixed and hydrodynamic lubrication are considered. Especially in mixed lubrication regime, dimples play an essential role on friction. Dimples serve as reservoirs for secondary lubrication phenomenon. In mixed lubrication regime, the lubricant in dimples permeates to the interspace of asperities, asperity contact decreases and film thickness becomes greater causing friction to decrease. GT32 type oil satisfies friction reduction more than the SAE30 type oil, since GT32 oil has a smaller viscosity. For optimum friction reduction, dimple size came out to be an important factor.

Figure 2.6 – Bearings with dimples [11]

Strand [2] made a similar study that investigates the groove design of a wheel loader bearing. These grooves can be considered as lubricant reservoirs, just like the dimples. Grooves also help the abrasive third bodies, like debris, to be removed from mating surfaces. Three bearing types; X-shaped, H-shaped and a bearing with no groove are compared. Profile measurements were made along the bearing length before and after tests. Strand recommends the measurements to be performed when the bearing is its housing. The form, waviness or roughness values differ, when the bearing is fit to the housing or is removed from the housing. As a measure for wear, area under wear-bearing length is taken into consideration. Bearing with X-shaped groove gave 29% more wear, and bearing with H-shaped groove gave 35% less wear with respect to the grooveless bearing.

Tevrüz stated that laboratory studies for fundamental tribological behaviors of polymers are generally performed in standard test rigs such as pin on disk or pin on ring types. However, having special geometric or kinematical characteristics, PTFE bearings should be tested in full-scale [12]. The tribological behavior of carbon filled PTFE bearings regarding different parameters such as sliding distance, bearing pressure and speed were investigated. The work is a full-scale experimental study. All the test procedures are strictly determined to eliminate potential practical errors in results. The steel shaft is selected as the mating member. The weight reduction and surface profile are measured for wear analysis. Wear and frictional characteristics came out to be dependent on load and velocity. For instance, the results show that friction increases as velocity increases, however the rate of increase slows down at higher velocities. Figure 2.7 shows that for any load or velocity value, the friction coefficient tends to converge a constant value with time. Wear rate reaches a stable value as well, but faster than friction coefficient does. This convergence phenomenon is attributed to the carbon / PTFE film transfer and adherence to steel shaft surface. Author commented as the temperature increase prevents PTFE composite films from being formed on surface by causing the filler material to be uncovered, which wears the shaft surface. Therefore, load and velocity dependence of wear and friction can be reduced by decreasing bearing temperature. Since friction coefficient results are more complicated, specific experiments, whose velocity or pressure scale is narrower for a particular application, are recommended to be performed.

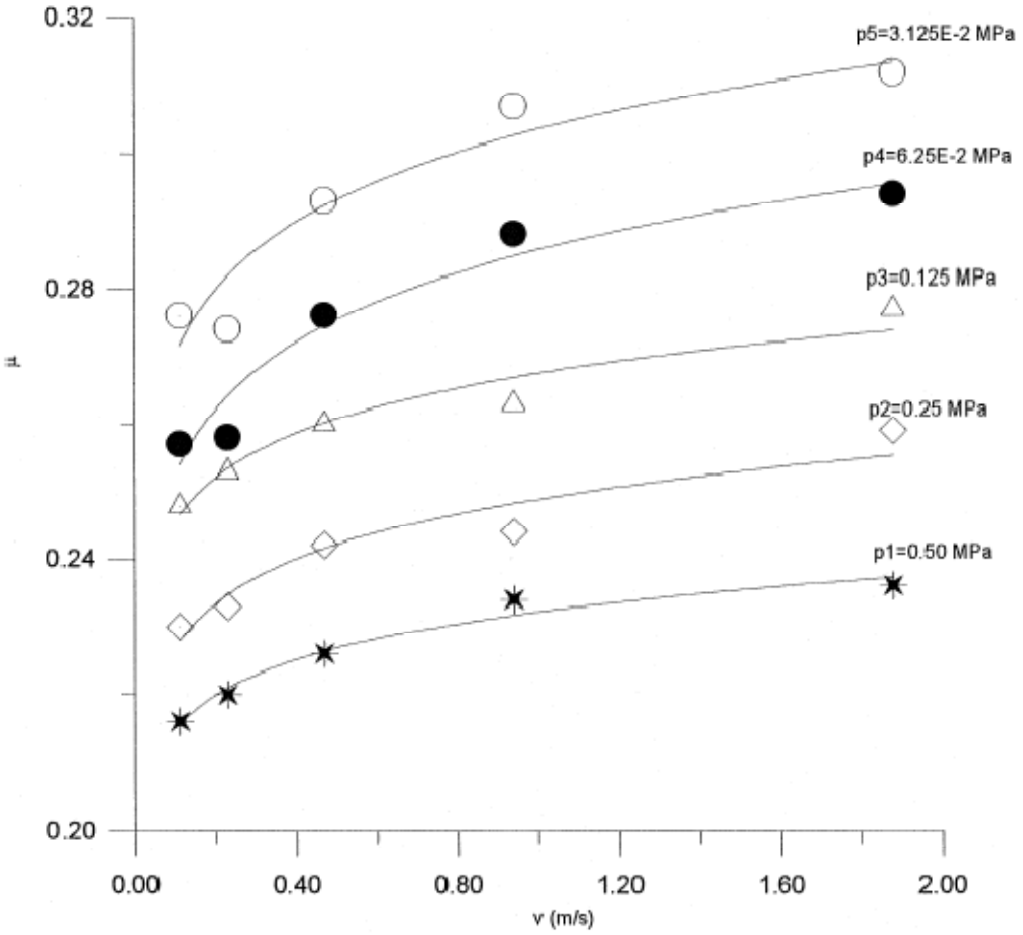

Figure 2.7 – Friction coefficient-velocity diagram for different pressure values [12]

There are test studies regarding the wear behavior of bearing materials, which can be performed not by full-scale bearings but with specimens of bearing materials. This approach is used when rapid tests are desired in order to make many tests in a short period of time.

Tamura et al. [13] studied the wear characteristics of WJ7 white metal, which is quite popular lining material in boundary lubricated bearings. A Φ200 mm shaft made up of JIS S45C steel is in contact with the lining material. The wear tests are performed under static and dynamic loads, created by a hydraulic cylinder, which is shown in

Figure 2.8. In dynamic loading, two different stress ratio (ratio of the maximum stress to the minimum stress) values, R = 2 and R = 10, are applied; where the stress, σ, is defined as the load per unit projected area of lining. In these dynamic tests, the shaft speed is constant at 287 rev/min. For statically loaded tests, different shaft speeds are also tried. Friction coefficient, μ, and temperature of specimen are recorded continuously. A test cut-off time, N_f, is defined according to the specimen width, as the previous studies showed a relationship between lining life and specimen width. The test results show that temperature increase rate of specimen increase as shaft speed increase and as R ratio

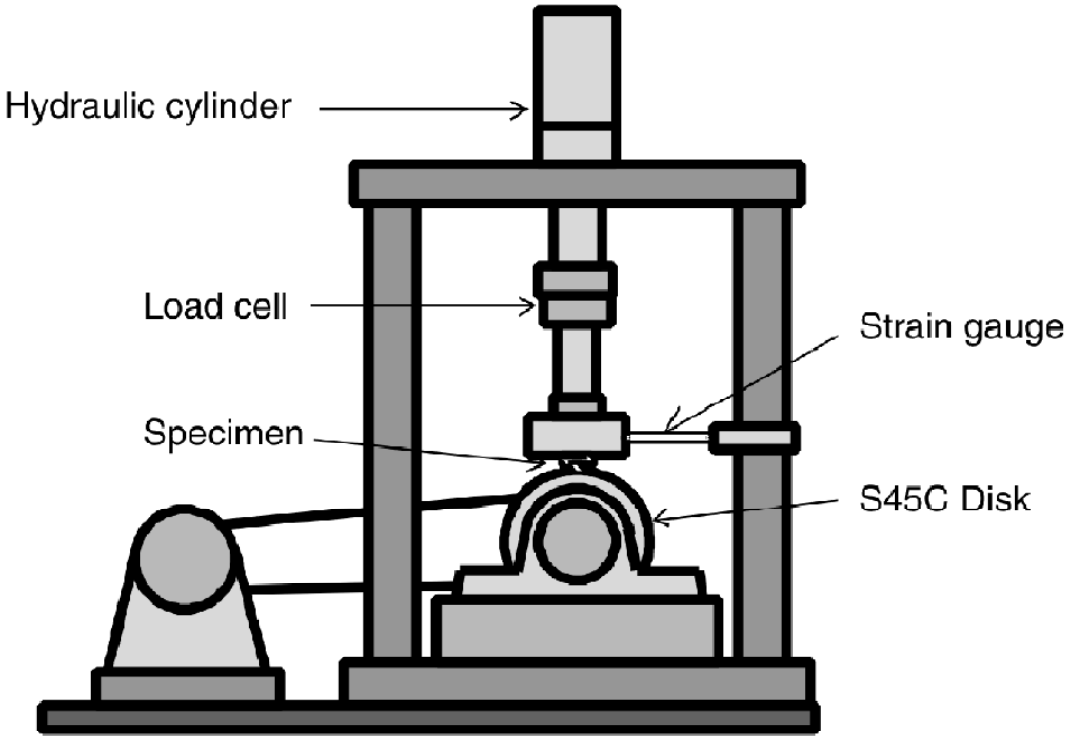

Figure 2.8 – Schematic illustration of the test machine [13]

converges to 1. Friction coefficient increases with shaft speed, but it is not affected considerably by maximum stress, as can be seen in Figure 2.9. A linear relationship is observed between cut-off life and maximum stress. Without depending the stress ratios, there is a unique relation between average stress and cut-off life. A shear stress, τ, is defined as $\mu.\sigma_{average}$. There observed to be a linear relationship between the shear stress and the cut-off life, regardless of shaft speed and R ratio. τ = 0.2 MPa is found to be a threshold value for failure occurrence.

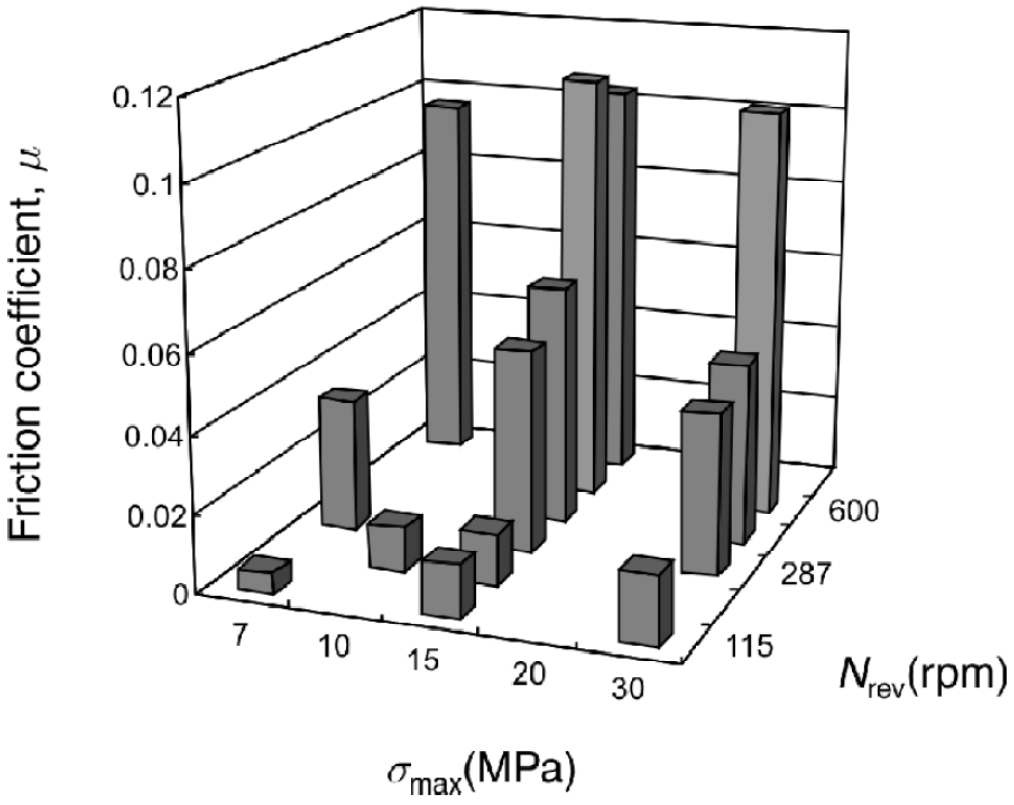

Figure 2.9 - Friction coefficient – maximum stress – shaft speed relation [13]

Bierlein et al. developed a test procedure for heat treated or coated surfaces and lubrication parameters [14]. A thrust washer and ring, shown in Figure 2.10, are used for mating surfaces. The procedure is based on pressure-velocity (PV) relationship of

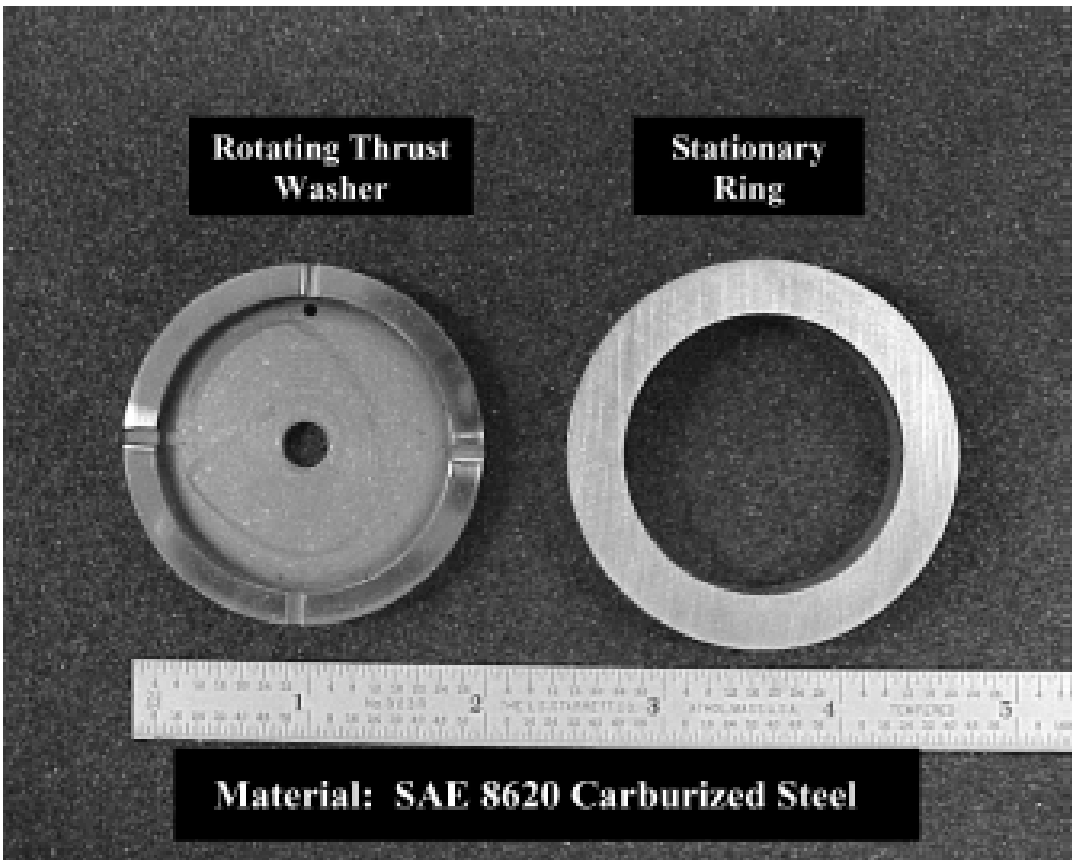

Figure 2.10 – Test washer and ring [14]

washers, which is also valid for journal bearings. PV factor is defined as the scalar multiplication of pressure and surface speed. It determines the heat input to the system, which is an important factor for frictional and wear characteristics of bearings. As a unit, 1 kPV is taken to be equal to 35 kPa.m/s. The test bench lets user perform rapid tests and measure parameters, such as temperature, friction; and

control pressure and velocity precisely. With the assumption of bearing failure at a constant PV, different test scenarios were performed. The tests were started at some velocity and zero pressure value; then pressure is increased gradually. These scenarios can be seen on Figure 2.11 with straight lines, showing the ISO-PV lines, as well. Tests are terminated when measured torque is observed to increase rapidly to an abnormal value. Different test plans ended with similar PV values, about 110 – 125 kPV; which is consistent with the initial assumption. Study proved that PV level approach satisfies the technical and business needs since different surface coatings, treatments and lubricant performance can be tested easily.

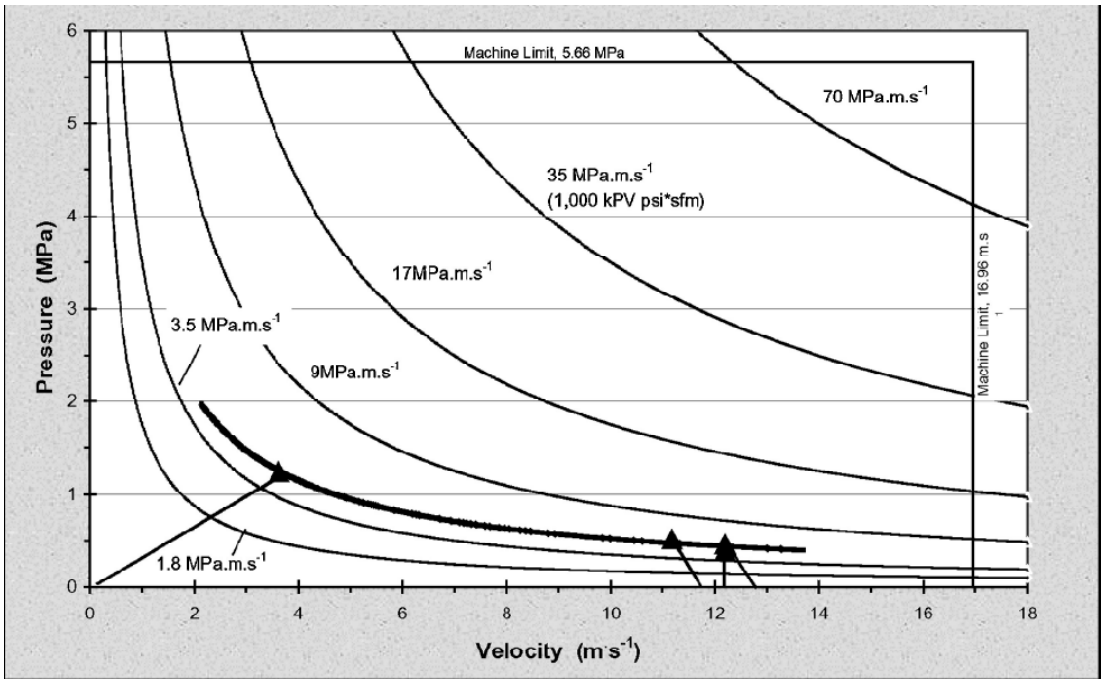

Figure 2.11 – ISO-PV curves and test scenarios [14]

Zhang et al. studied the scuffing behavior of engine piston pin / bore bearing in mixed lubrication [15]. A test bench, capable of simulating real conditions of engine

piston pin, is set up. Many parameters such as torque, velocity, temperature, friction coefficient are recorded. Bores having different surface parameters are tested. After tests and surface examinations, a scuffing model is developed. According to tests, for areas where mild wear occurred, originally rough bore resulted in more material flow and tearing, and thus more accumulated debris. Similarly, on severe wear regions, increase in roughness value is observed to shorten the time for scuffing outset. From SEM micrographs, cyclic load is found out to help scuffing initiation. Cyclic loads results in fatigue cracks, or sometimes plastic deformation, and thus material transfer becomes very easy. The developed criterion states that scuffing occurs when maximum surface tangential traction, τ_{sm}, is larger than the modified shear strength, S_m (2.3). An uncertainty factor, f^*, is introduced for the effects of elements that affect wear and scuffing and modeling inaccuracy.

$$f^* = \frac{\tau_m^*}{S_m^*} \tag{2.2}$$

where τ_{sm}^* and S_m^* are the critical values of τ_{sm} and S_m, which correspond to the maximum asperity temperature when scuffing starts. It is observed that scuffing uncertainty factor is proportional to maximum asperity temperature stemming from frictional heating, coefficient of friction and surface roughness. Effect of radial clearance on f^* is not linear; the trend is similar to change in minimum film thickness.

Hiraoka [16] studied the friction and wear life mechanism of oscillating journal bearings. Performance of bonded MoS_2 lubricant is tested in different conditions. Load, oscillation angle, velocity are the parameters. Tests are performed in air and vacuum chamber, shown in Figure 2.12. Before tests MoS_2 is sprayed to both bearing and shaft, after a sand blasting process. Test duration is limited by the rapid increase of friction coefficient. Friction coefficient in vacuum came out to be lower than that in air. Results are shown in Figure 2.13. In both vacuum and air conditions, lubricant film thickness is retained up to failure and decrease rapidly. Pitting is observed

before the failure; many pitting holes are formed by partial film debonding near the substrate of coating.

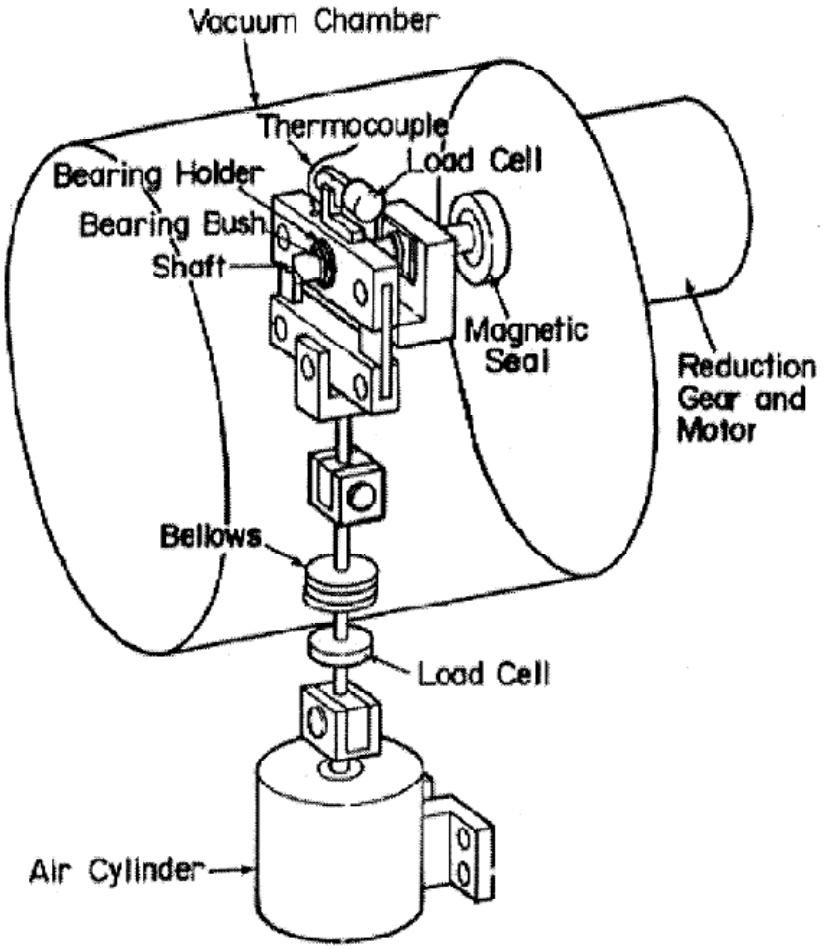

Figure 2.12 – Test setup with vacuum chamber [16]

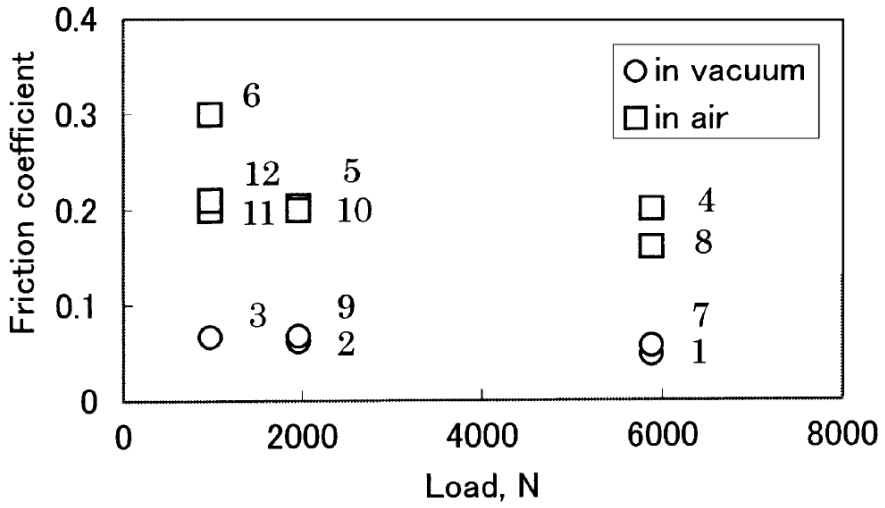

Figure 2.13 – Friction coefficient at different load values [16]

There are test methods published by International Organization for Standardization, regarding the metal bearing material selection [17]. These methods let one try different material or lubricant combinations for bearings running repeatedly or for long periods under boundary lubrication. These are pin-on-disc and block-on-ring tests.

Marklund and Larsson simulated a wet clutch system on a pin-on-disc test rig [18]. A stationary pin is axially loaded towards a rotating disc, as shown in Figure 2.15. Disc velocity and pin force are under control and temperature at the pin tip is measured. Friction force can be calculated from the torque output of motor rotating the disc. Friction is described as functions of temperature and sliding speed. To do this, a surface is fitted to test results, as can be seen in Figure 2.14. Friction coefficient is not greatly affected by temperature. At 30°C, the maximum difference in friction coefficient is about 5% between different loads, indicating an opportunity to simplify the friction coefficient function because a sufficiently accurate friction coefficient can be described as only a function of sliding velocity and interface temperature. The method is stated to be time saving and cheap with respect to the traditional methods,

especially when different combinations are desired to be tested, but not a final test method for clutch design.

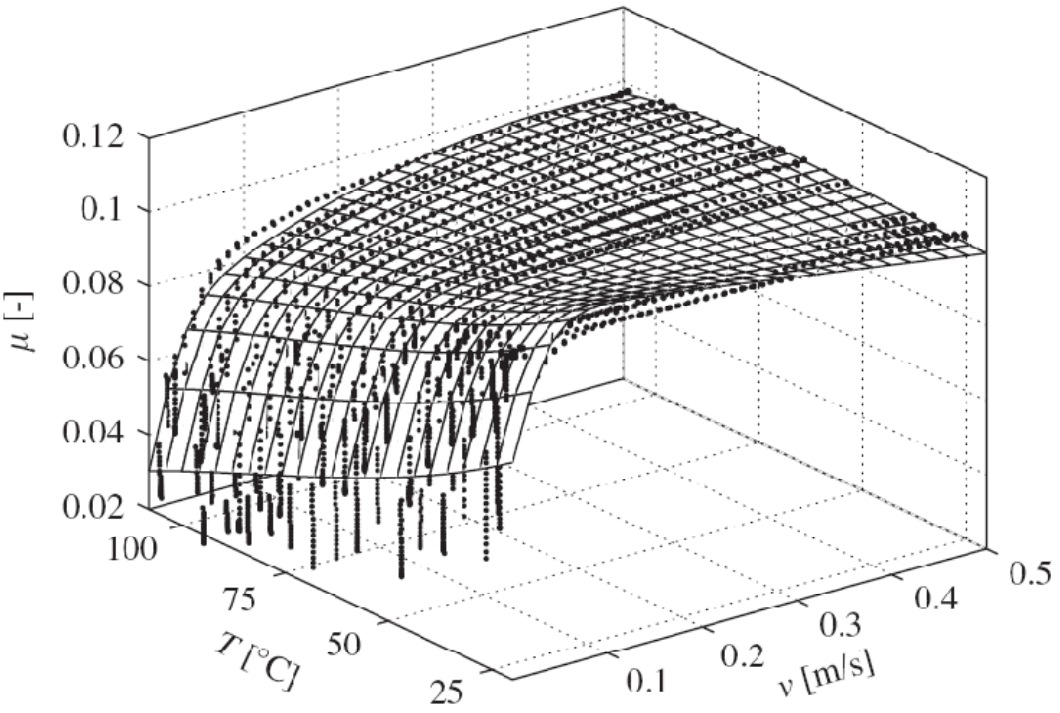

Figure 2.14 – Measured data and the approximate mathematical surface [18]

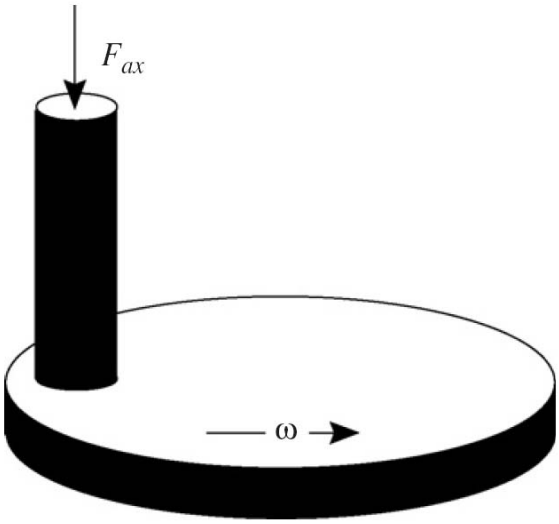

Figure 2.15 – Pin-on-disc test schematic [18]

A block-on-ring type study is performed by Koszela et al. The effects of surface texturing on anti-seizure properties of a steel-bronze assembly are studied [19]. The test method and setup lets one perform many tests in a short period of time. Bronze blocks having different surface textures, mainly dimples, are exposed to constant load and unidirectional sliding on steel ring, as can be seen in Figure 2.17.

Figure 2.16 – An example of dimpled blocks [19]

Seizure criterion was based upon friction coefficient and temperature, which were monitored continuously. Eight different textures were tried, each by three tests. 3-D surface topography was mapped. Pit to total area ratio was observed to be an important parameter for seizure. As this ratio goes above an optimum level, load bearing capacity of the block is diminished.

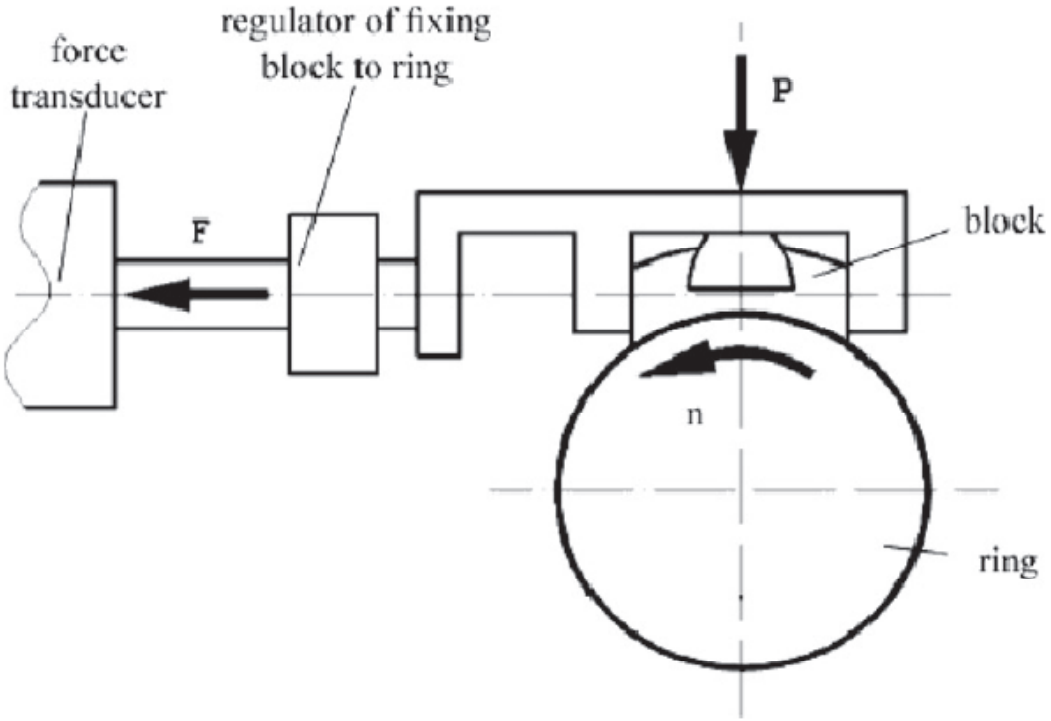

Figure 2.17 – Schematic of test setup [19]

A similar test type is the ball-on-disc test. This time instead of a static pin, a ball is pushed on a disc. Siu et al. investigated the effect of surface roughness and coating thickness on friction and wear behavior of MoS_2 metal coating [20]. An AISI 52100 bearing Φ9 mm steel ball was slid on AISI 440C steel coated with MoST (MoS_2 / titanium composite) under pure sliding with oil lubrication. Ball initial roughness is

0.01 μm in tests. Discs having different surface roughness values from R_a = 0.01 - 1 μm are tried. Loads and sliding speeds are varied from 5 to 50 N from 0.1 to 4.5 m/s respectively. Wear rates and friction coefficients are recorded, and maps regarding these two results are formed. Friction coefficient map can be seen in Figure 2.18. Map is divided into three regions according to the surface roughness values. Solid lines are the constant friction coefficient values, arrows direct through the increasing friction coefficients. From R_a = 0.01 to 0.05 μm, coating thickness hugely affects the friction, they are inversely proportional. But roughness is not a significant factor on friction in this region, as can be seen. As surface roughness increases above 0.05 μm, friction becomes dependent both on coating thickness and roughness. Over R_a = 0.02 μm, friction depends only on surface roughness and effect of coating thickness is negligible. Wear, whereas, came out to be independent of coating thickness. Surface roughness value is ineffective on wear below 0.1 μm. After 0.1 μm, as surface roughness increases, wear rate also increases.

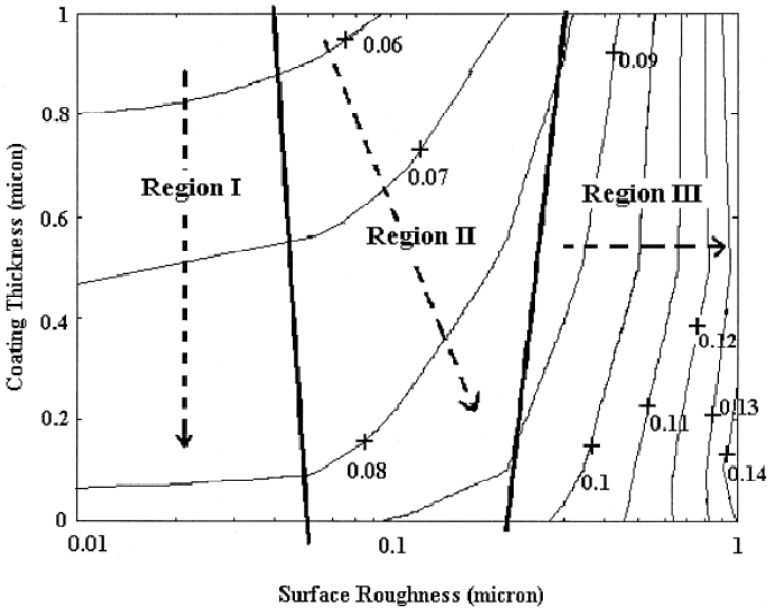

Figure 2.18 – Friction coefficient map [20]

CHAPTER 3

WEAR ANALYSIS OF RUBBING BEARINGS

Wear is defined as the loss of substance from a solid body surface in frictional conditions, which appears as a gradual decrease of body dimensions and/or change of shape [3]. Wear may occur in different forms according to the nature of a process. Generally, most forms of wear occur at the asperities at the real area of contact, which are the high points of surfaces in a very small scale, like in Figure 3.1 [21].

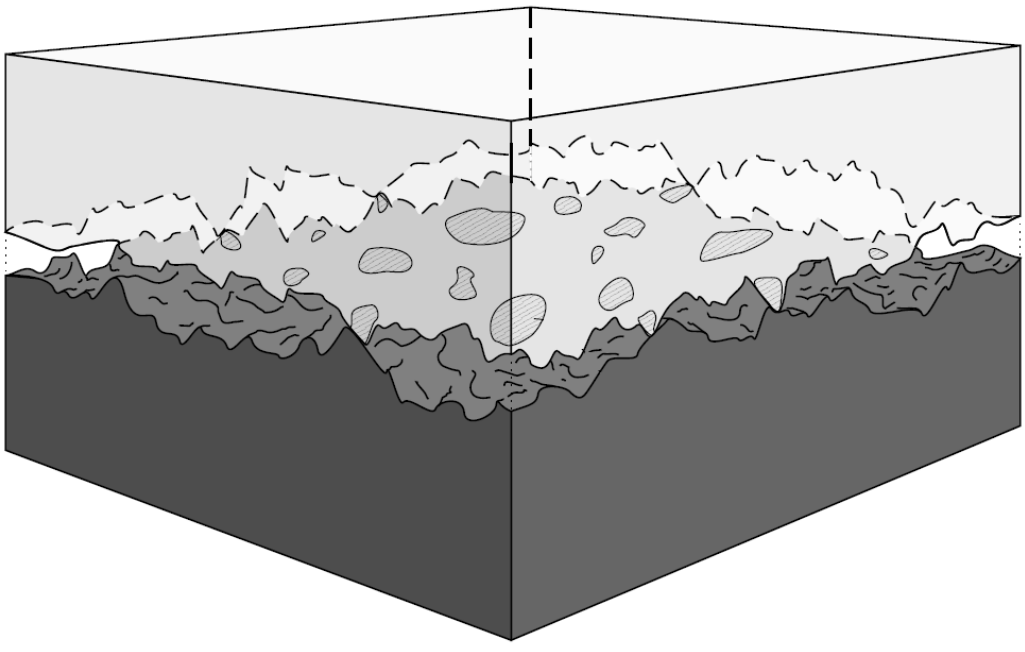

Figure 3.1 – Real contact of surfaces [21]

3.1. Wear Types

Wear can be classified into groups according to the nature of the occurring mechanism:

- **Abrasive wear:** Abrasive wear is the wear type when a hard solid removes material from a softer surface.

- **Adhesive wear:** Adhesive wear is the material transfer due to localized bonding between contacting solid surfaces. After formation of welding, shearing of welded junctions occurs because of the relative motion and material is removed.

- **Erosive wear:** Erosive wear is the material removal from a surface by a high-speed fluid flow or a stream of hard particles in a fluid flow. Cavitation in a fluid flow leads to the collapse of low-pressure gas bubbles on solid surfaces and particle erosion. If the particle is hard and solid then it is possible that a process similar to abrasive wear will occur. Where liquid particles are the erodent, abrasion does not take place and the wear mechanisms involved are the result of repetitive stresses on impact [21]

- **Fretting:** Fretting is a form of adhesive wear when two surfaces move with small oscillatory motion with respect to each other. It results in two forms of damage; surface wear and deterioration of fatigue life. The surface appears as pitted and fine powdered debris is observed. Gear teeth and wire ropes are common examples where fretting occurs.

- **Surface fatigue:** Surface fatigue occurs when a surface is subject to a sequence of compressive and tensile stresses. These stresses lead to cracking under surface and release lumps of material from surface. Phenomenon is commonly observed when a concentrated load passes over a surface, such as loaded ball or roller [8].

The dominant wear mechanisms occurring at excavator bearings are abrasive wear and adhesive wear. These two types are given in detail next sections. Erosion or cavitation is not observed since there is no fluid flow or particle stream in joints. For fretting small oscillations are required but because of the nature of excavator utilization, large movements occur instead of small repetitive oscillations. Contact stresses in earthmoving bearings are too small for causing cracks, since bearings are case hardened to a critical depth.

3.1.1. Abrasive Wear

Abrasive wear is the loss of material by the passage of hard particles over a surface. These particles may either be asperities of solids or individual grits trapped between surfaces. It occurs whenever a solid object is loaded against particles of a material that have equal or greater hardness. There are almost always several different mechanisms of wear, all of which have different characteristics [21]. These are cutting, fracture, fatigue and grain pull-out.

Cutting, occurs when a hard particle embeds in a softer material and because of the motion, soft material is removed from the path of hard particle as wear debris. In cutting mechanism, another phenomenon, called ploughing, may occur. This is defined as the wedge built-up in front of the moving hard particle. In studies, ploughing is found out to be less efficient than cutting in terms of metal removal rate [21].

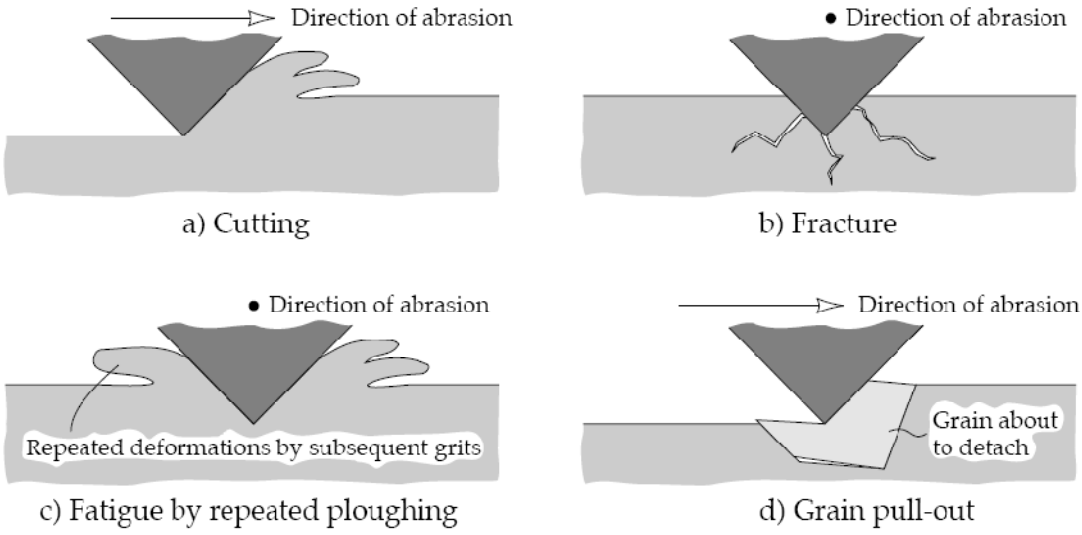

Figure 3.2 – Different mechanisms of abrasive wear [21]

Fracture, occurs especially when the abraded material is brittle. When asperities move successively across the surface, the accumulation of cracks can result in the release of large quantities of material. Brittle fracture is favored by high loads acting on each asperity, sharp edges on the asperity, as well as brittleness of the substrate.

Fatigue is caused by the repeated strain caused by grits deforming the area on the surface of a material. Mechanism is the sideways displacement of material and the subsequent fracture, as shown in Figure 3.2-c. Wear by repeated sideways displacement of material would also be a relatively mild or slow form of abrasive wear since repeated deformation is necessary to produce a wear particle.

Grain detachment or pull-out is a relatively rare form of wear which is mainly found in ceramics. This mechanism of wear can become extremely rapid when inter-grain bonding is weak and grain size is large.

Abrasive wear may occur in two-body or three-body modes. In two-body mode, grits are rigidly fixed to the sliding body, as in Figure 3.3. They pass over the surface like

a cutting tool. In three-body mode wear, grits are free to roll or slide on the soft surface, as in Figure 3.4. Investigations show that two-body wear is ten times faster than three-body wear, since the latter has to also compete with other mechanisms such as adhesive wear [21]. The worn material is not removed by a series of scratches as is the case with two-body abrasive wear. Instead, the worn surface displays a random topography suggesting gradual removal of surface layers by the successive contact of grits.

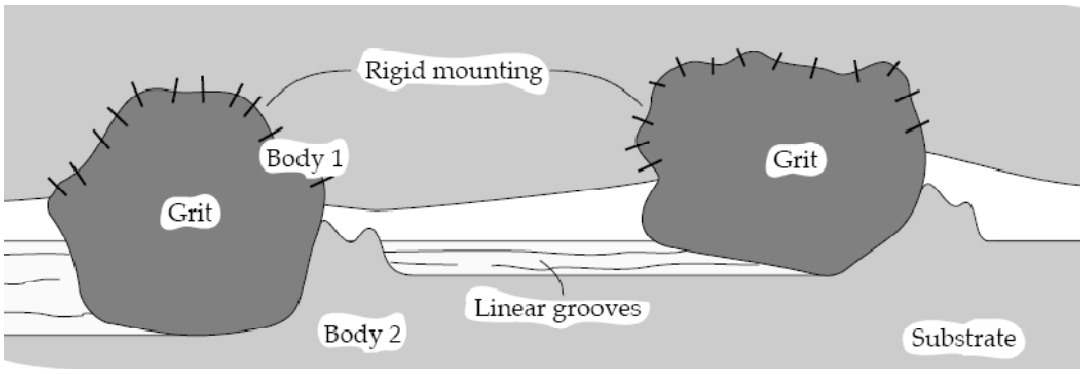

Figure 3.3 – Two-body abrasive wear [21]

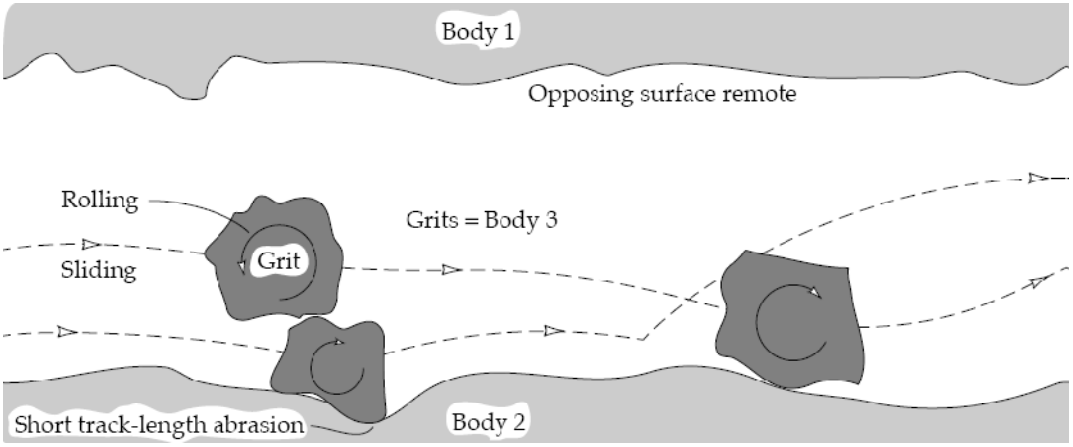

Figure 3.4 – Three-body abrasive wear [21]

3.1.2. Adhesive wear

Adhesion is the material transfer between two solid bodies in contact. Adhesion of metals is explained by electron transfer between contacting surfaces. Numerous free electrons are present in metals and on contact electrons may be exchanged between the two solids to establish bonding. The electrons are not bound by a rigid structure and providing that the distance between two bodies in contact is sufficiently small, i.e. < 1 nm, they can move from one body to another. As a result the electrons can bond two solids despite their differing atomic structures. In this sense, like materials tend to adhere more. Besides, adhesion is reduced with increasing surface roughness or hardness of bodies.

Adhesion shows itself as a wear type on running surfaces. Even sliding motion may be prevented by large friction coefficients or seizure. Most of the metals have oxide or contaminant layers on their surfaces in nanometric scales. This layer prevents adhesion of solids in normal contact. Therefore, adhesion tests are performed in clean vacuum chambers, where no oxide layer is formed. These tests show that adhesion –or separation- force is greater than the contact force, showing the effect of adhesion on friction coefficient.

Adhesive wear occurs by shearing and cracking of soft material under the pressure of hard asperity in motion. After the bonding realizes, soft material fractures in a ductile or brittle way, as can be seen in Figure 3.5.

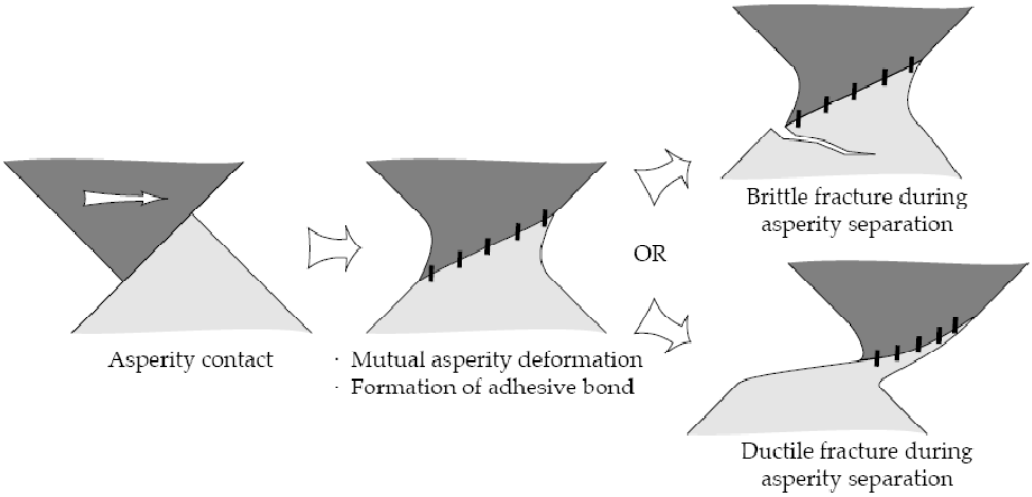

Figure 3.5 – Model of deformation in adhesive asperity contact [21]

An important concept in adhesive wear is the transfer film. The particle abraded from soft material can stick to the hard material with a strong bond permanently. These stuck particles form a transfer film throughout the surface. These transfer particles are generally harder then the substrate material due to work hardening during plastic deformation. Therefore, after forming of the film, transfer particles may wear its own source substrate. Transfer particles are usually the same size as the area of real contact which suggests that just a few transfer particles are carrying the load. In some cases, transfer particles can grow and lead to seizure of sliding surfaces. However, not all transfer layers are undesirable. Some PTFE based materials and solid lubricants are used in the contact surfaces of bearings to form a transfer layer since they have low friction coefficient.

3.2. Wear Calculation

Different wear models were developed in history, from simple theories to complex methods. As theories get more complex, more parameters are involved and number of assumptions increase.

A simple and useful method, especially used in experimental studies is Archard's method. Method states that total wear volume is proportional to the real contact area, A_r, times the sliding distance, s:

$$V_{wear} = KA_r s = K\frac{F}{H_{soft}}s \tag{3.1}$$

where real contact area is defined as force, F, per hardness of softer material, H_{soft}. The usefulness of equation in experimental studies comes from easy measurement of the parameters force, sliding distance, wear volume or hardness. Scientists do not have to deal with the shapes or distribution of asperities, which are difficult to observe, but rather have a general approach to the phenomenon.

Hardness is defined as the ability of a material to resist plastic deformation when a force is applied. Different scales or units are used for indicating hardness, such as Rockwell, Brinell or Vickers. Since wear is the plastic deformation and consequent removal of asperities, surface hardness value is an important parameter for wear. Archard's theory assumes that harder material wears the softer one. Therefore, in the wear equation hardness of the soft material exists.

The coefficient K, is called the wear coefficient and determines the severity of wear. It depends on surface or material properties of both materials and surrounding media. Wear coefficient is generally a transient value, since some factors affecting wear changes in time. The clearest examples are the temperature increase with friction and surface roughness decrease with the removal of asperities.

Another concept in life determination specific for journal bearings is the PV limit. PV value is the multiplication of pressure on bearing and the linear speed between pin and bearing; its unit is MPa.m/s. Pressure is taken as the force per unit projected are of bearing. Since both pressure and velocity are good control variables in terms of measurement and accuracy, life of journal bearings are given in their PV capacities. PV is also a measure of heat dissipation capability of a journal bearing.

PV is obtained by expressing the Archard equation in another way. Dividing equation (3.1) by projected area of the bearing:

$$\frac{V_{wear}}{A} = \frac{K}{H_{soft}} \frac{F}{A} s \tag{3.2}$$

Assuming a uniform wear throughout the bearing width wear depth, h, can be defined as the critical dimension change, and V being the sliding distance per unit time:

$$h = \frac{V_{wear}}{A} \ , V = \frac{s}{t} \tag{3.3}$$

Equation (3.2) becomes:

$$\dot{h} = \frac{K}{H_{soft}} PV \tag{3.4}$$

Equation 3.4 shows that wear rate depends on a coefficient determined by the metal pair and if exists lubricant, and the PV value which can be considered as a design criterion for a particular case. PV calculation for oscillating bearings is given in Appendix C.

The pressure value in PV concept is based on the projected area of bearing. However, actual pressure distribution on a cylindrical contact is a function of angle

throughout the contact, as shown in Figure 3.6. For a stable and measurable wear phenomenon at excavator joints, no plastic deformation has to be observed in macro scale. For a closed cylindrical contact of same materials, this can be checked by the pressure and stress distributions, given by Ciavarella et al. [22]. E, ΔR, Q being the Young's modulus, bearing radial clearance and load per unit pin length, respectively; the half contact angle, ε, can be found from equations (3.5), (3.6), (3.7).

$$b = \tan\left(\frac{\varepsilon}{2}\right) \tag{3.5}$$

$$\frac{E\,\Delta R}{Q} = \frac{2}{\pi} - \frac{1-b^2}{b^2} - \frac{I_b}{b^2\pi^2(1+b^2)} \tag{3.6}$$

$$I_b = \int_{-b}^{b} \ln\frac{\sqrt{(b^2+1)}+\sqrt{(b^2-t^2)}}{\sqrt{(b^2+1)}-\sqrt{(b^2-t^2)}}\frac{dt}{1+t^2} \tag{3.7}$$

Pressure distribution, p(y), through the contact for any angle ϕ yields as

$$\frac{R_2\,p(y)}{Q} = \frac{2}{\pi\sqrt{(b^2+1)}}\frac{\sqrt{(b^2-y^2)}}{1+y^2} + \frac{1}{2\pi b^2(1+b^2)}\ln\frac{\sqrt{(b^2+1)}+\sqrt{(b^2-y^2)}}{\sqrt{(b^2+1)}-\sqrt{(b^2-y^2)}} \tag{3.8}$$

$$y = \tan\left(\frac{\phi}{2}\right) \tag{3.9}$$

Where ϕ is defined in Figure 3.7.

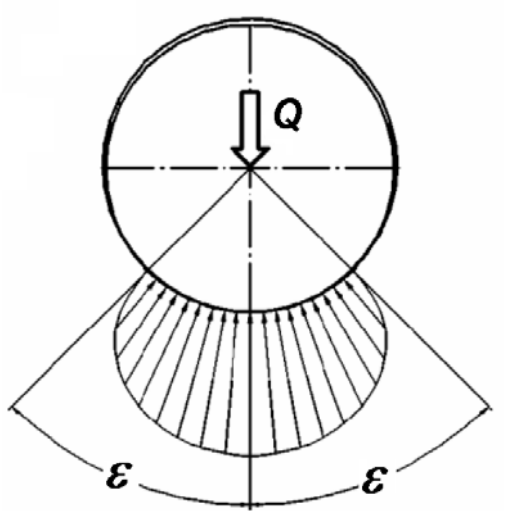

Figure 3.6 – Pressure distribution on the pin [8]

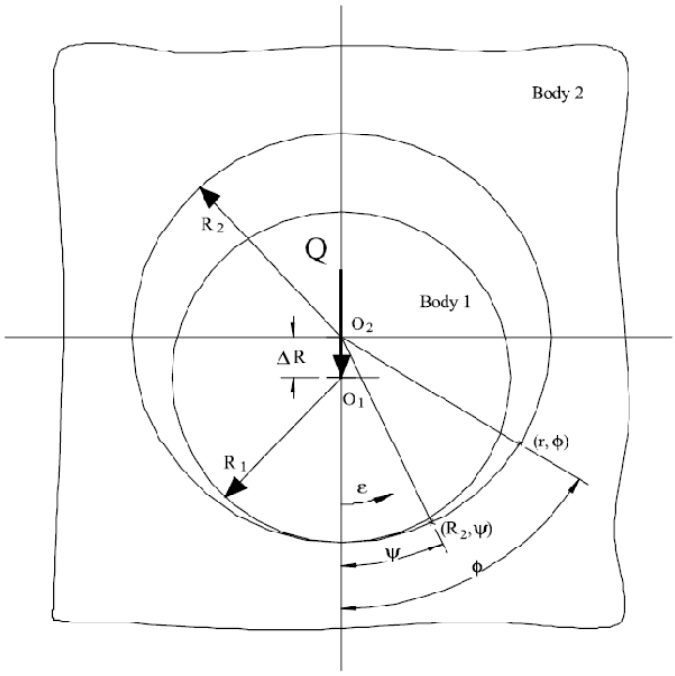

Figure 3.7 – Closed cylindrical contact – symbols [22]

R_2 being the bearing inner radius, shown in Figure 3.7, a change of variables is applied.

$$q(y) = \frac{p(y)R_2}{Q} \tag{3.10}$$

Stress field can be calculated as in equations (3.11) and (3.12).

$$-\sigma_r + \sigma_\theta = \frac{1}{\pi}\int_{-\varepsilon}^{\varepsilon} q(\psi)d\psi + 2\int_{-\varepsilon}^{\varepsilon} q(\psi)L_1 d\psi + \frac{3-\upsilon_2}{2\pi\rho}\cos\phi \tag{3.11}$$

$$\sigma_r = \frac{\rho-1}{2\pi\rho}\int_{-\varepsilon}^{\varepsilon} q(\psi)d\psi + \int_{-\varepsilon}^{\varepsilon} q(\psi)L_2 d\psi + \frac{3-\upsilon_2}{4\pi}\frac{\rho^2-1}{\rho^3}\cos\phi \tag{3.12}$$

where $\boldsymbol{\upsilon_2}$ is the Poisson's ratio of the bearing, and

$$L_1 = \frac{1}{2\pi}\frac{1-\rho^2}{\rho^2 - 2\rho\cos\theta + 1} \tag{3.13}$$

$$L_2 = \frac{1}{2\pi}\frac{(1-\rho^2)^2}{\rho}\frac{\cos\theta - \rho}{(\rho^2 - 2\rho\cos\theta + 1)^2}, \quad \theta = \psi - \phi \tag{3.14}$$

$$\rho = \frac{r}{R_2} \tag{3.15}$$

CHAPTER 4

DESIGN OF AN EXPERIMENTAL SET-UP FOR BEARING WEAR TESTS

Wear is a mechanical failure type, which depends not only on the material properties, but also on the operating conditions, the surface properties and the presence of third or fourth bodies. The most important disadvantage of wear for analytical modeling is that it occurs in micro-scale, especially for boundary lubrication case. The best way to predict wear properties is to carry out experiments under the same operating conditions. In this study, a test bench was set up for wear simulation in excavator attachment joints.

4.1. Design Requirements for Bearing Test Set-up

The test bench has to simulate the operating conditions of the 22-ton excavator whose boom foot bearing is to be studied. The load and speed of the test bench is the main parameters in the design stage. The boom foot bearing is exposed to about maximum 230 kN force and the maximum angular speed is about 20°/s. Therefore, a test set-up is to be designed to apply about 230 kN force at a speed of 25°/s.

The auxiliary parts, which are required for the test but do not affect the results directly, were selected as the ones in the real excavator application. The bearing housing and dust seal are the examples of these parts.

4.2. Description of Bearing Test Set-up

A test bench was designed and constructed for the wear tests. The bench is made up of mainly an oscillating arm on which the test bearing to be mounted through a fixed pin. A test housing, into which the test bearing is fitted, is mounted to the oscillating arm by bolts and can be detached whenever desired. Different sizes of bearings can be tested with the help of auxiliary parts.

The oscillating arm is driven by a hydraulic system to get the required high forces. An electronic unit, which gets position data from hydraulic cylinders, controls the pressure in the system. By this way, a real force – motion diagram on an excavator can be simulated. In order to prevent knocking in the hydraulic system, proportional control is utilized.

On the test bench, the arm can oscillate between ±45°. Bearings up to 140 mm in diameter and 200 mm in length can be tested. All the parts are made of St-52 steel.

4.3. Mechanical Construction of Bearing Test Set-up

The test bench mechanism consists of a fixed base, an oscillating arm, a fixed pin, the test bearing, auxiliary guides and two hydraulic cylinders. The components of bearing test bench are shown in Figure 4.1. Some important dimensions of test bench is given in Appendix A.

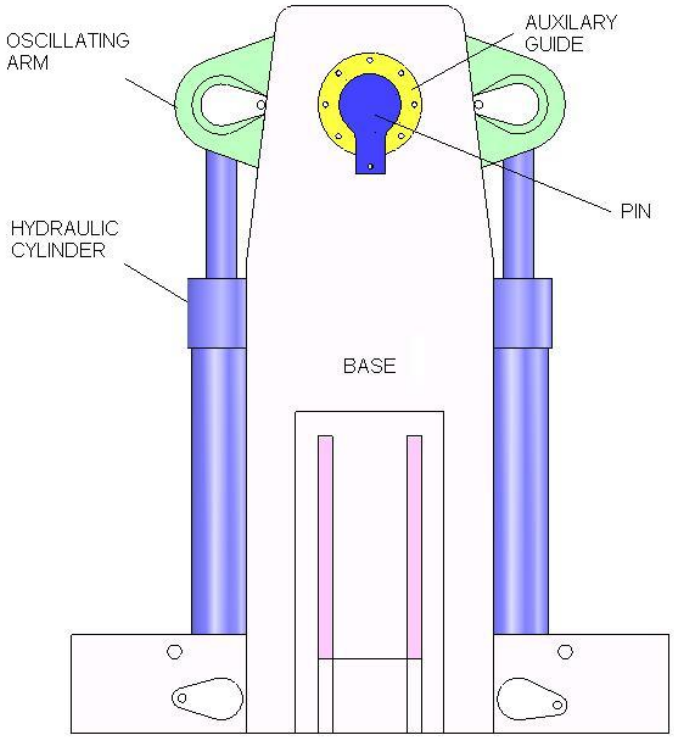

Figure 4.1 – Components of bearing test bench

- **Base**: The base accommodates the arm, pin, test housing and hydraulic cylinders. It is mainly for the fixation of mechanism to the ground.

- **Oscillating Arm:** This part accommodates the test bearing at the middle through the fixed pin, which is connected to the base. The two hydraulic cylinders with revolute joints at the rod ends are connected to the arm. While the bench is testing, the oscillatory motion is satisfied on this part.

- **Test Bearing Housing:** The test housing accommodates the test bearing. The housing is fixed to the oscillating arm by bolts on the flange, as shown in Figure

4.2. Therefore, the test bearing rotates together with the oscillating arm. The bearing housing is selected as the original one used in excavator booms. The housing is shown in Figure 4.3.

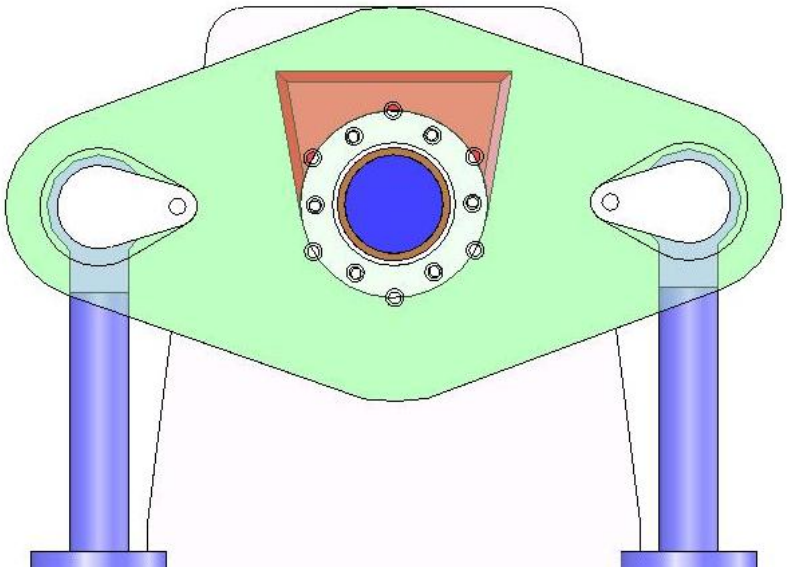

Figure 4.2 – Arm cross-sectional view

Figure 4.3 – An end view of the test bearing housing

- **Hydraulic Cylinders:** The hydraulic cylinders excite the motion on the test bench. The cylinders are connected to the base and the rods are connected to the oscillating arm with revolute joints. A control unit drives the hydraulic cylinders automatically. The rod and pipe diameters are Φ60 and Φ100 mm, respectively. The engineering drawing of hydraulic cylinders is given in Appendix A.

- **The Pin:** Pin is the part where test bearing mates. It is fixed to the base from its lug, as shown in Figure 4.4. It connects the oscillating arm and the housing to the base. The diameter, surface properties and the material of the pin are selected as the original one mounted to excavators. A Φ8 mm hole is drilled from the end

to the mid-section of pin for surface temperature measurement close to the test bearing. A thermocouple is placed at the end of the hole. The engineering drawing of the test pin is given in Appendix A.

- **Auxiliary Guides:** These guides, shown in yellow in Figure 4.4, are for testing bearings of different sizes of bearings in width and/or diameter. A different sized guide can be mounted to the base for different sized bearings.

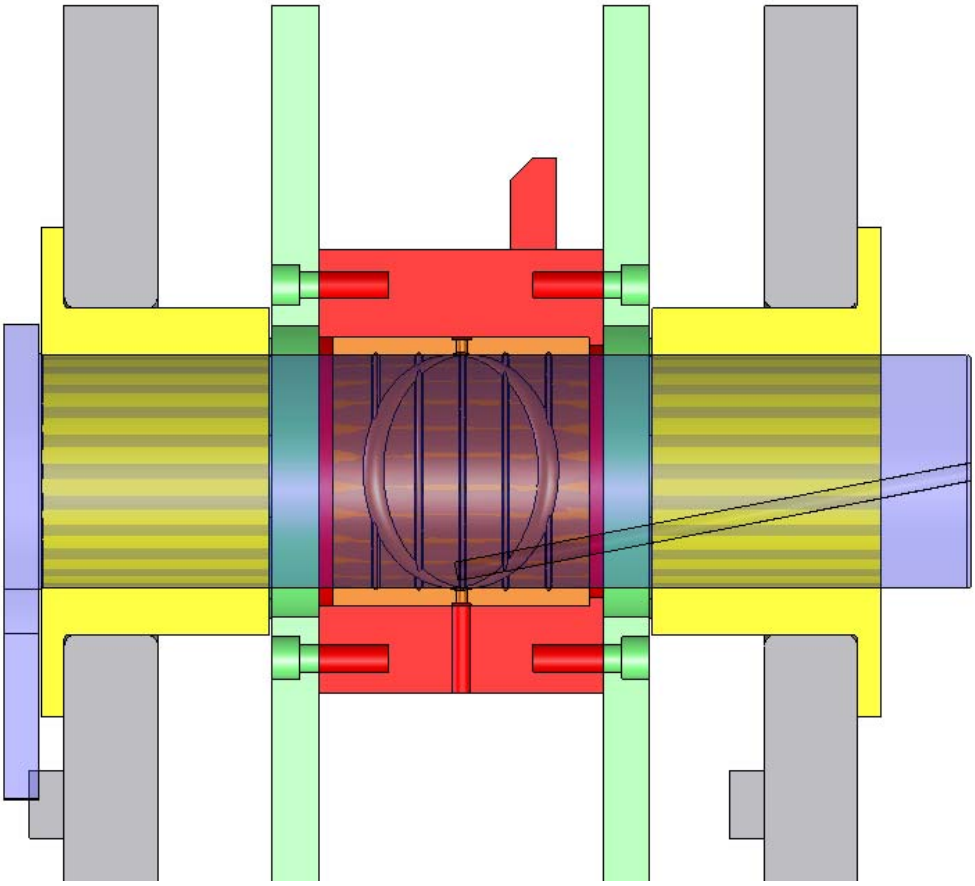

Figure 4.4 – Pin cross-sectional view
(Pin is shown as transparent for indicating details)

4.4. Operating Principle of Variable Bearing Load

When starting the test, the bottom sides of both hydraulic cylinders are pressurized with the same value. Since the net moment on the oscillating arm with respect to the test bearing center is zero, the rotation of the arm does not occur. Afterwards, the topside of one of the cylinders is pressurized with relatively lower pressure value with respect to that of the bottom side. At the same time, the topside of the other cylinder opens to the tank of the hydraulic system. By this way, the moment equilibrium is lost, and the arm rotates to one side. During rotation, the force on bearing is not lost, since the pressure value in the bottom sides of the cylinders is much higher than that in the topsides.

When the stroke length finishes, the topside of the other cylinder is pressurized and, the topside of the first cylinder is decreased to the tank pressure. This time, the direction of rotation changes and the oscillating motion is obtained.

The hydraulic pressures and motion is driven by a hydraulic control system. During one stroke, the pressure at the bottom sides is adjusted by the control system, according to the length of one of the cylinders. By this way, the magnitude and direction of forces that occur on an excavator attachment joint can be simulated.

4.5. Hydraulic System for Variable Bearing Loading

Whole power system consists of two different open-center hydraulic systems, as can be seen in Figure 4.6. One system, to be called “pressure line”, satisfies the high pressure at the bottom of both cylinders. The pressure value here is varied in order to simulate the real bearing forces. The other system, to be called “motion line”, controls the oscillation movement and speed of test by pumping the oil to the topsides of the cylinders successively. The cylinder position is fed back to the control system by a linear variable differential transformer (LVDT) as shown in Figure 4.5.

Thus, the ends of stroke and speed can be determined, and the bottom pressure can be adjusted according to the cylinder position.

Figure 4.5 – Linear variable differential transformer mounted on oscillating arm

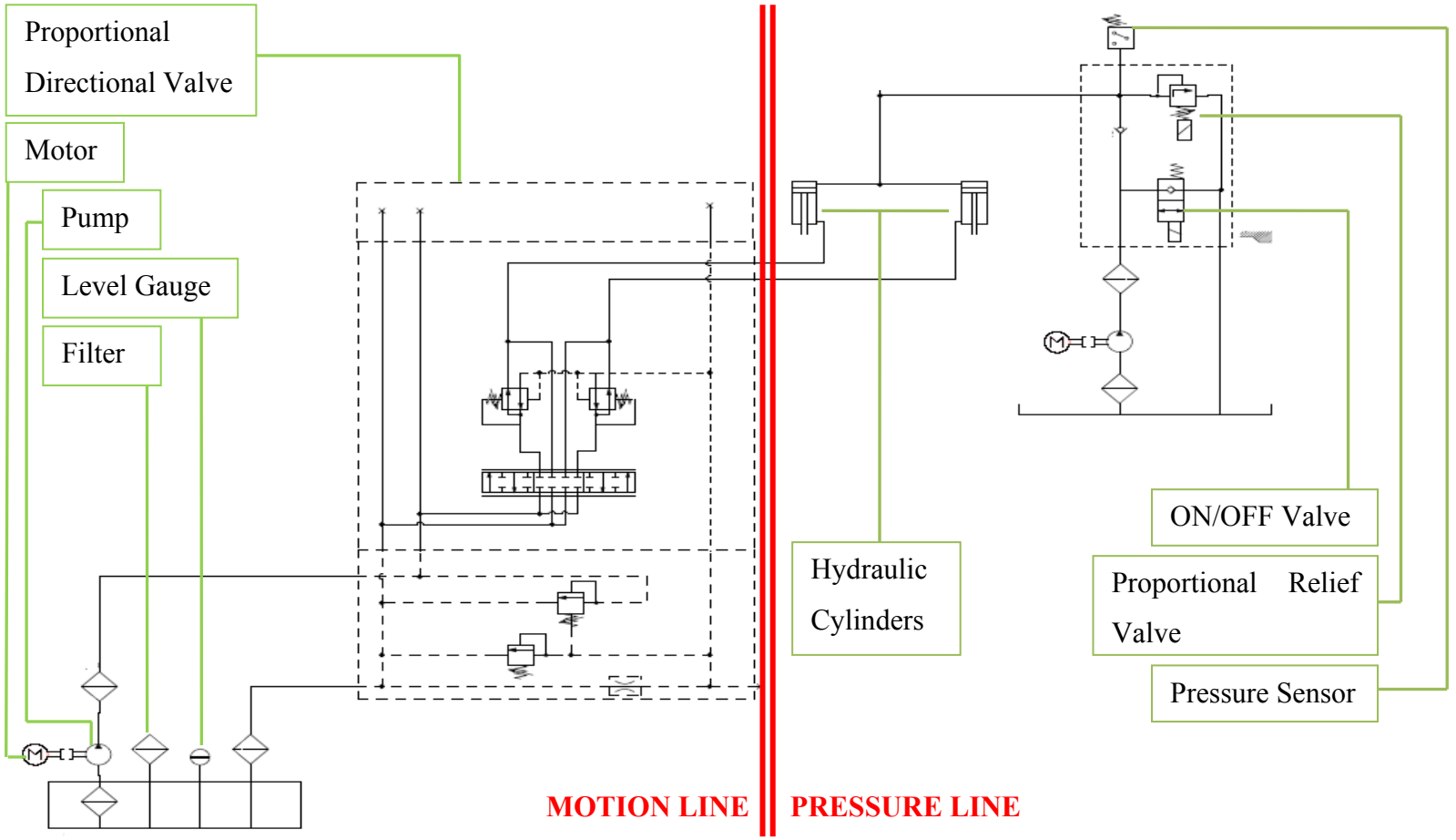

Figure 4.6 – Schematic of hydraulic power pack

The pressure line on the hydraulic system consists of a 2.2-kW electric motor, a constant displacement pump, a proportional pressure relief valve, an ON/OFF valve, a pressure sensor, a hydraulic accumulator and filters, as shown in Figure 4.7. Basically, the oil pumped is relieved from the proportional pressure relief valve to the tank, and thus, the desired pressure is satisfied at the bottom sides of hydraulic cylinders. While the cylinders are moving, the hydraulic oil just displaces from one cylinder to another; there is no flow from cylinder to the tank. This lets the pressure be adjusted without large amount of oil transportation in the hydraulic system. A pressure sensor sends the pressure data to the control system. The filters keep the hydraulic circuit clean against dirt or tiny particles. There is an analog manometer, and a manometer test point for digital pressure measurement.

The motion line on the hydraulic system, shown in Figure 4.7, consists of a 7.5-kW electric motor, a constant displacement pump and a proportional directional valve consisting of sections. The inlet section has oil inlet lines and pressure compensators for damping of sudden pressure peaks. It also determines the maximum working pressure of the valve. The middle section is the part, which directs the hydraulic oil to the cylinders. It is an electro-hydraulically operated valve, having two solenoids that hold the spool in the desired position. Keeping this spool in the right position at the right cylinder lengths satisfies smooth running of the system. When the oil is pumped to one of the cylinders, the oil from the other cylinder returns back to the tank.

The hydraulic oil heats up while the system runs because of viscous friction. Hence, an oil cooler is installed to the system, which is shown in Figure 4.8. The cooler pump sucks the oil from tank and pumps through the cooler to the tank again.

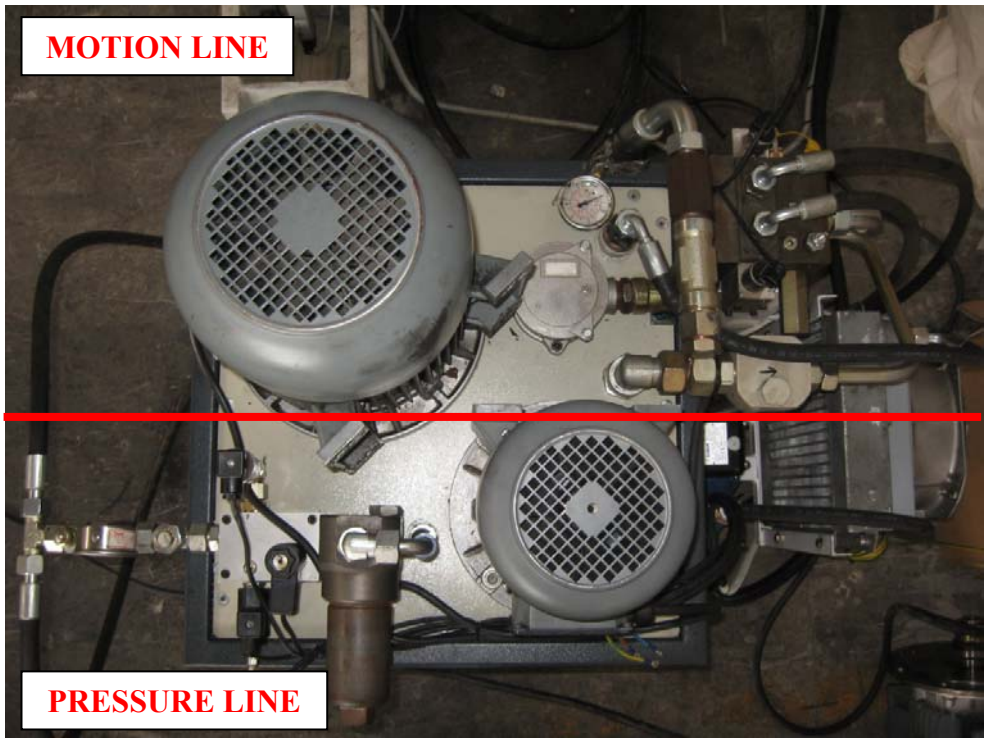

Figure 4.7 – A top view of hydraulic power pack

Figure 4.8 – A view of hydraulic power pack oil cooler

4.6. Control System for Hydraulic Circuit

Speed, operating range and pressure profile of the test can be adjusted by the control system. These parameters are determined before tests and can be entered to the control panel. In the test, control system receives cylinder length position data from LVDT, and sends electric current to the valves accordingly. Hence, the desired motion is satisfied.

The control panel, shown in Figure 4.9, is a touch screen where the input parameters are entered or monitored. In “Settings” menu, the hydraulic pressure and velocity spectrum throughout a cycle is entered. The oscillation angle is determined also in this setup. “Test Control” menu lets one start, pause or finish a test. From “Test Screen” menu, the pressure, velocity and angle values of the test can be followed. Also, the current level on a valve can be seen instantly. The test time and the current number of cycles are monitored here. “Manual Control” menu lets one bring the hydraulic cylinders to a desired position manually. This is important especially when installing a new housing for a new test.

A view of whole test equipment can be seen in Figure 4.10.

Figure 4.9 – A view of control panel

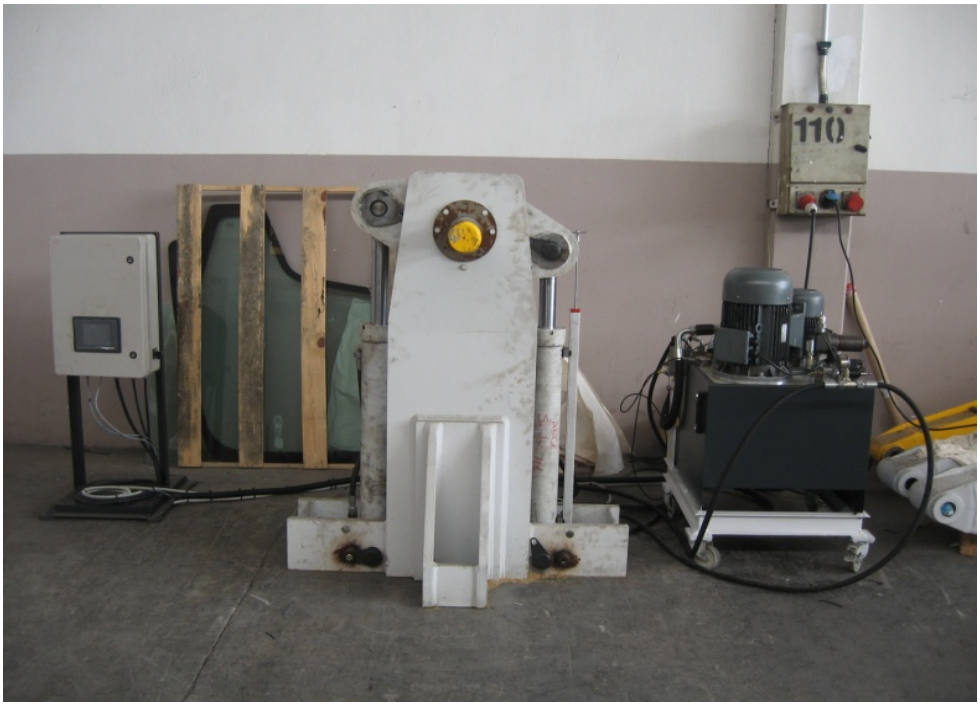

Figure 4.10 – Test bench with hydraulic power pack and control panel

CHAPTER 5

BEARING WEAR TESTS AND MEASUREMENTS

5.1. Properties of Test Components

The test bearing was selected as the boom foot bearing of 22-ton excavator, shown in Figure 5.1. The inner and outer diameters are 100 and 115 mm, respectively, the width is 110 mm. It is made of 16 MnCr 4 steel, hardened to 54 HRC by carburizing. There is a black-colored manganese phosphate coating on the bearing, which has oil retaining properties in its porous structure to improve frictional properties. Coating is corrosion resistant, as well. There are circular and helical grooves for grease storage.

Figure 5.1 – A view of steel bearing

Another bearing as an alternative to the steel bearing was also tested. It is a cast bronze bearing having graphite plugs. While bronze material bears the heavy load, graphite satisfies the lubrication as a solid lubricant. Bronze alloy of the bearing contains aluminum, manganese and iron, as well. It has a hardness of about 25 HRC. The bearing is shown in Figure 5.2.

Figure 5.2 – A view of bronze bearing

A steel bearing without grooves was also tested. All material properties and tolerances are the same with the standard steel bearing. There is only a radial groove at the half width of the bearing. This bearing can be seen in Figure 5.3.

Figure 5.3 – The grooveless steel bearing

The test bearings are press-fitted to the housing in such a way that the oil channel in the housing is at the same distance to the two oil holes on the bearing. The position is shown in Figure 5.4. By this way, grease is compelled to fill the pin-bearing clearance not from one hole, but from the two holes with the same amount.

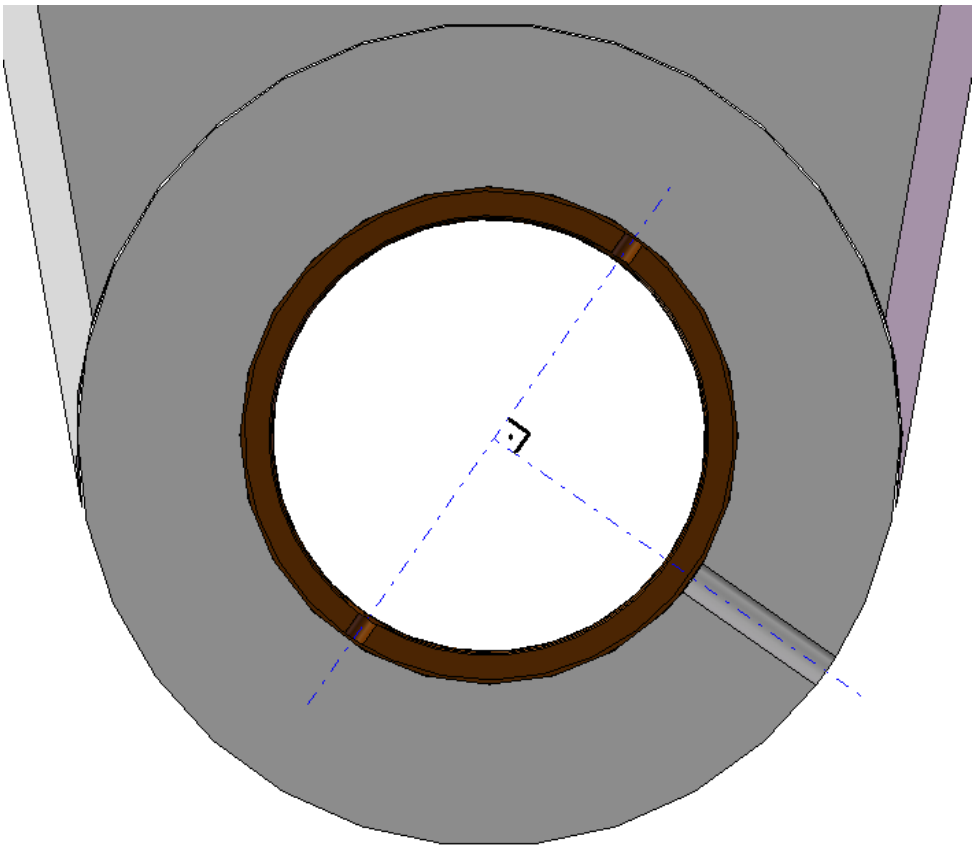

Figure 5.4 – Angular positions of the oil holes in the test bearing and in the housing

The test pin material is AISI 4140 with a core hardness of 27 HRC. The pin is induction hardened to a surface hardness of 58 HRC. It has a surface roughness of 0.5 μm R_a. A view of test pin is shown in Figure 5.5.

Diametral clearance between pin and bearing varies from 0.192 mm to 0.420 mm, while the corresponding range for the bronze bearing is 0.108 – 0.197 mm.

For the grooveless steel bearing test, a modified pin is used. Two grease channels were machined on the pin in the axial direction. These channels are 90° apart from each other and on the loaded half of the pin. The channels help bearing to be greased at all times. The modified pin can be seen in Figure 5.6. The engineering drawing is given in Appendix A.

Figure 5.5 – A view of test pin

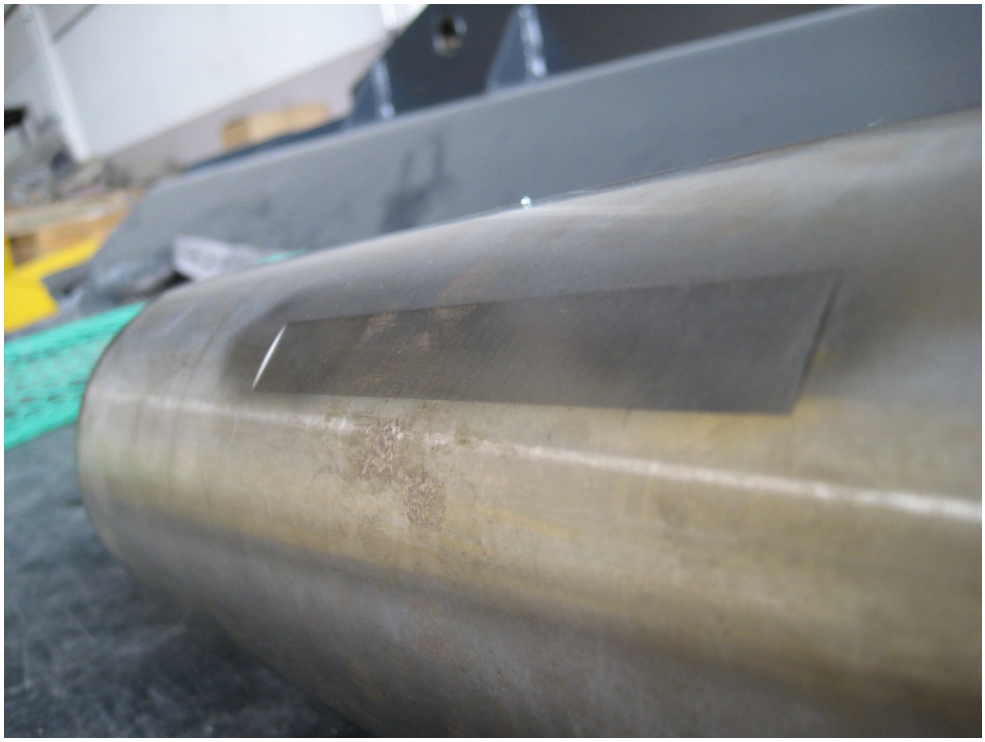

Figure 5.6 – The channel on the modified test pin

5.2. Test Procedure

In the tests, the oscillating motion with an intended force profile was realized. From the force analysis of a standard digging operation on an excavator, a force-time graph is obtained. The profile of this graph is shown in Figure 5.7. The force given in the test was selected to have a similar trend with the real value. The force applied in test bench deviated from the actual force profile; however, the difference is small enough to perform healthy tests. Keeping the trend in Figure 5.7, the tests were performed with different maximum force values. Force on the test pin is obtained from hydraulic pressure values. The calculation is given in Appendix B. In load cycles, the same region of the bearing of the bearing was always exposed to the highest force.

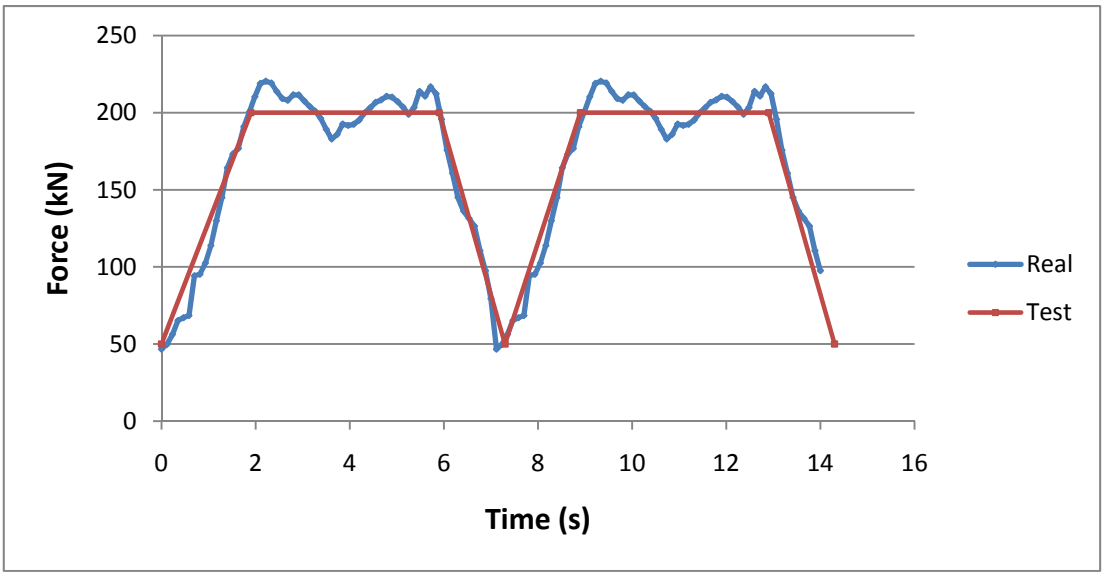

Figure 5.7 – Force – time graph formed in one digging cycle

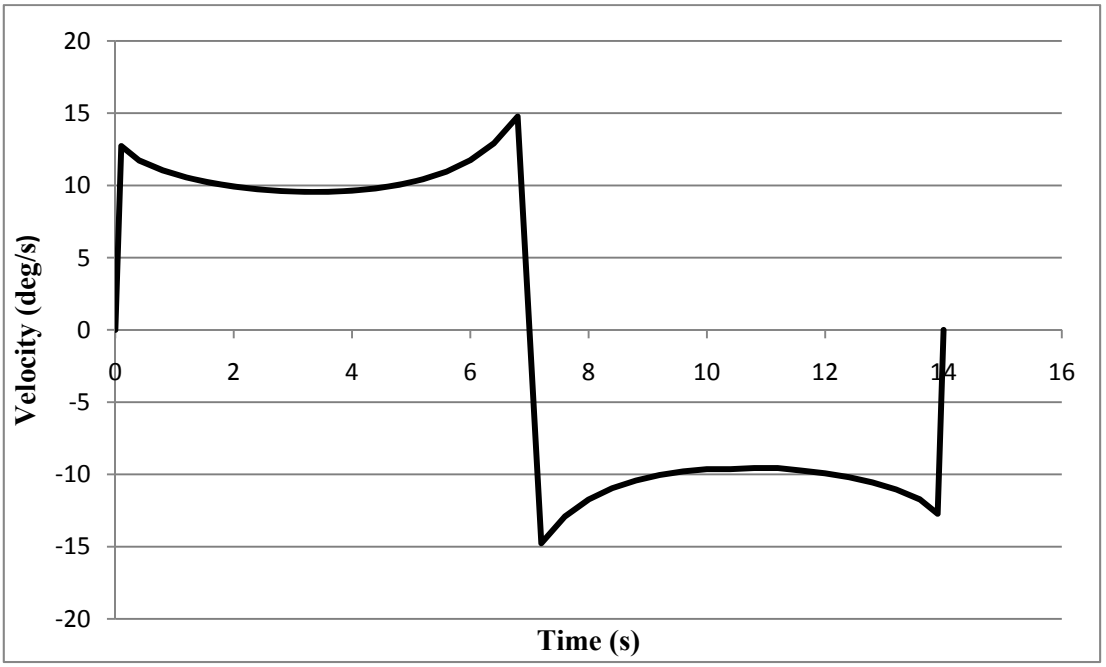

Figure 5.8 – The velocity-time graph corresponding to 14 s/cycle

Different tests were performed with different loads and velocities given in Table 5-1. The resulting PV values are also given in Table 5-1, which are calculated according to the methodology in Appendix C. The oscillating motion was in the range of ±45°. The velocity input is almost a step input, shown in Figure 5.8. At t=0, the position of bearing with respect to the pin can be thought as corresponding one of the oblique lines that deviate by β from the vertical line, shown in Figure C.1.

During the tests, the steel bearings were lubricated with 20 grease gun strokes of lithium grease in every hour. The bronze bearings were not lubricated.

Table 5-1 – Data for the tests performed

Test	Bearing Type	Number of Cycles at Failure	Pressure on Bearing (MPa)	Period (s/cycle)	PV (MPa.m/s)
1	Steel	2007	23.0	14	0.26
2*	Steel	9028	15.1	14	0.17
3	Steel	3710	24.9	14	0.28
4	Steel	900	24.9	14	0.28
5	Steel	330	24.9	14	0.28
6*	Steel (No Groove)	16446	18.2	7	0.41
7*	Bronze	16500	18.2	7	0.41
8*	Bronze	82030	21.0	7	0.47

*No seizure

5.3. Wear Measurements

Wear determination is based upon the dimensional and characteristic change of mating surfaces. The test bearing dimensions are measured by a coordinate measuring machine having an accuracy of 0.1 μm. The wear measurements on the bearing are performed while the bearing is fit in the housing, since the bearing elastically expands and the dimensions change when the bearing is got out of the housing [2]. The predefined tracks on the bearings are scanned with the CMM before and after the tests; the dimensional difference between the measurement profiles gives the depth of wear.

Two types of measurement are performed on the test bearings. Two axial measurements are taken; one from the lines where the bearing is exposed to the maximum pressure and the other is from the diametrically opposite line where the bearing is not loaded as shown by the dashed lines in Figure 5.9. Since no wear is expected on the unloaded region, the opposite line measurement is used as a reference surface for removing the offset between the measurements before and after the tests.

Six circular measurements are taken from each region, which is separated by circular grooves as shown in Figure 5.9. The wear depth throughout the half circumference in the loaded region is measured. 180° rotation of CMM probe inside the bearing can not be obtained for all circular measurements. However, the minimum arc of 90° about the maximum pressure line can be scanned in those cases.

In every measurement, CMM creates a reference and the dimensions are displayed with respect to this reference. Therefore, some surfaces were machined on the housing for CMM to locate the reference, as shown in Figure 5.10. The reference surface is at the center point of bearing hole on one surface; hence it is determined by two holes on flange surface, which were drilled equidistantly from the bearing center. The x and y axes are determined with respect to these holes. The z-axis alignment is normal to the flange surface; which is determined by the 3 points on the flange. This flange was ground to 0.005 mm tolerance for precise alignment of z-axis in every measurement.

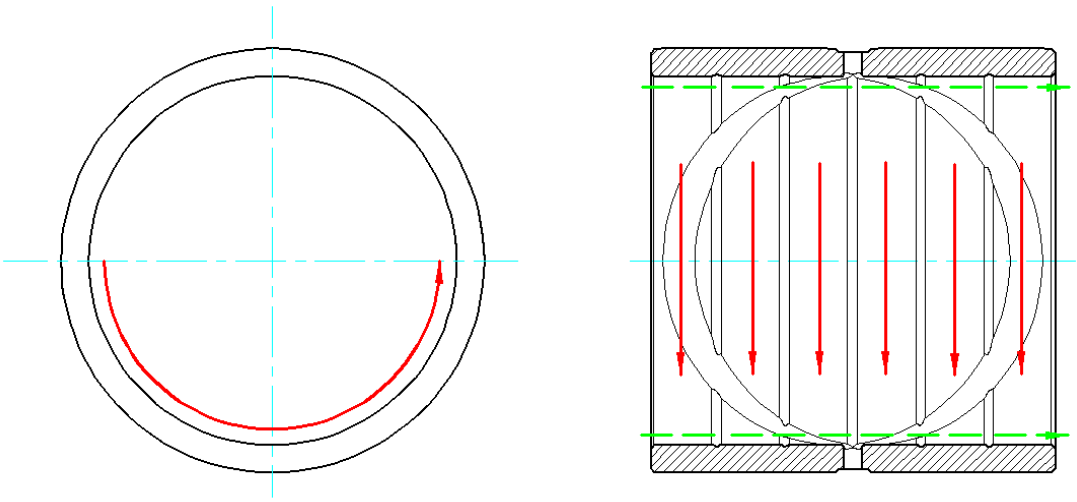

Figure 5.9 – Measurement tracks on the test bearing surface

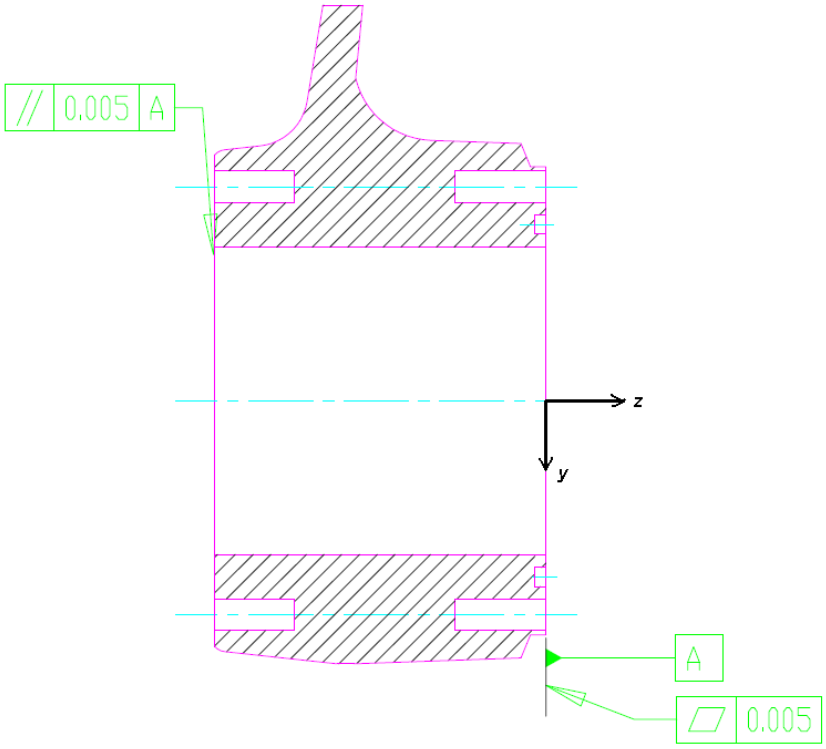

Figure 5.10 – Flatness and parallelism tolerances of the test bearing housing side surfaces

CHAPTER 6

DISCUSSION AND CONCLUSIONS

In this study, wear tests of the boom foot bearings of 22-ton excavators are performed in order to determine the wear characteristics of pin-bearing pairs. Firstly, a test rig was designed and constructed for the study. It is considered that the rig should simulate the actual operating conditions as close as possible and should let the user to test bearings of different size, as well. Some tests were conducted and wear results were compared.

6.1. Pressure Distribution on the Steel Test Bearing

The pressure distribution on the steel bearing can be calculated by the method given in section 3.2. The input parameters for the test bearing are given in Table 6-1.

Table 6-1 – The input parameters for the steel test bearing

c	Diametral clearance	0.42 mm
Q	Load per unit length	2581 N/mm
E	Elastic Modulus	210 GPa
R_2	Inner Radius of Bearing	50.15 mm

For the parameters given in Table 6-1, the pressure distribution over the steel bearing is calculated. The maximum pressure (σ_r), maximum tangential stress (σ_θ) at contact surface and the contact angle come out to be 90 MPa, -50 MPa and 42.6°, respectively. This pressure value is far below the yield strength of bearing and pin materials; therefore no plastic deformation is observed. The distribution is shown in Figure 6.1, whose notation is given in Figure 3.6. This graph can also be regarded as the wear depth rate distribution for constant velocity according to the equation (3.4). The calculation is available for only steel test bearing, since the theory is valid for similar materials.

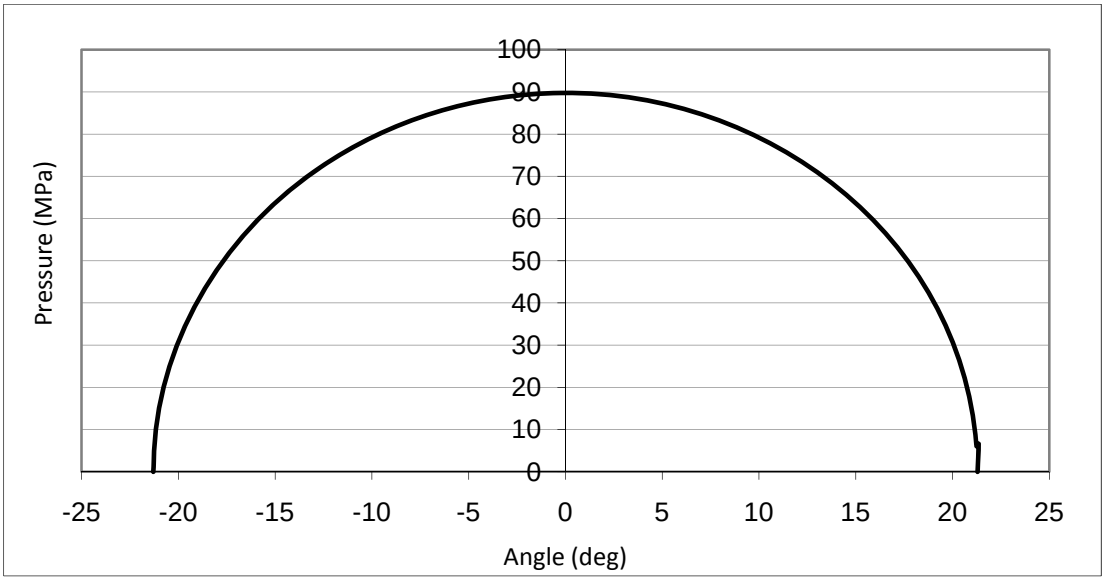

Figure 6.1 – The pressure distribution on the test bearing

6.2. Discussion of Test Results

Eight tests were performed totally. Six of them were performed with steel bearings and the other ones were performed with bronze bearings. The parameters and results of the tests are given in Table 6-2. In the first test, lubrication period of the steel bearing was selected to be 4 hours, which is the same as the current recommended lubrication period of excavator bearings. However, seizure occurred nearly in 2.5 hours and test was ended. Other steel bearings were lubricated in every hour.

Table 6-2 – Parameter and result data of the tests

Test No:	Bearing Type	Mean Pressure on Bearing (MPa)	Period (s/cycle)	PV (MPa.m/s)	Number of Cycles at Failure	Wear Volume (mm^3)
1	Steel bearing	23.0	14	0.26	2007	Seizure
2	Steel bearing	15.1	14	0.17	9028	12.46
3	Steel bearing	24.9	14	0.28	3710	Seizure
4	Steel bearing	24.9	14	0.28	900	Seizure
5	Steel bearing	24.9	14	0.28	330	Seizure
6	Steel bearing (No groove)	18.2	7	0.41	16446	55.39
7	Bronze bearing	18.2	7	0.41	16500	265.5
8	Bronze bearing	21.0	7	0.47	82030*	-

* Test did not end

The tests were ended if seizure occurred. Other tests were not ended due to any failure. When the number of cycles reached a much higher value than the previous ones, it is decided to finish the tests.

Standard steel bearings, which are currently used in the machines, are numbered 1 to 5 in Table 6-2. At high PV values, standard bearings gave poor results, and seizure occurred before reaching considerable amount of cycles. This phenomenon is

observed to be very unstable, since it occurred in a wide range of cycle values. The forth and the fifth bearings are seized in very low cycle values. Therefore, there might be some other effects other than PV factor in these tests such as dirt or debris. The seizure region on the steel bearings was observed between the mid-section and the side of the bearing. Since this behavior is asymmetric with respect to the mid-section, non-uniformity in contact is thought to occur during tests. The seizure occurred on the same half of the bearing. The seizure region in the bearing is shown in Figure 6.2.

The third test was performed with a PV value higher than the first test. However, the seizure occurred later than the first test. The increase of lubrication amount increased the seizure time but did not prevent seizure.

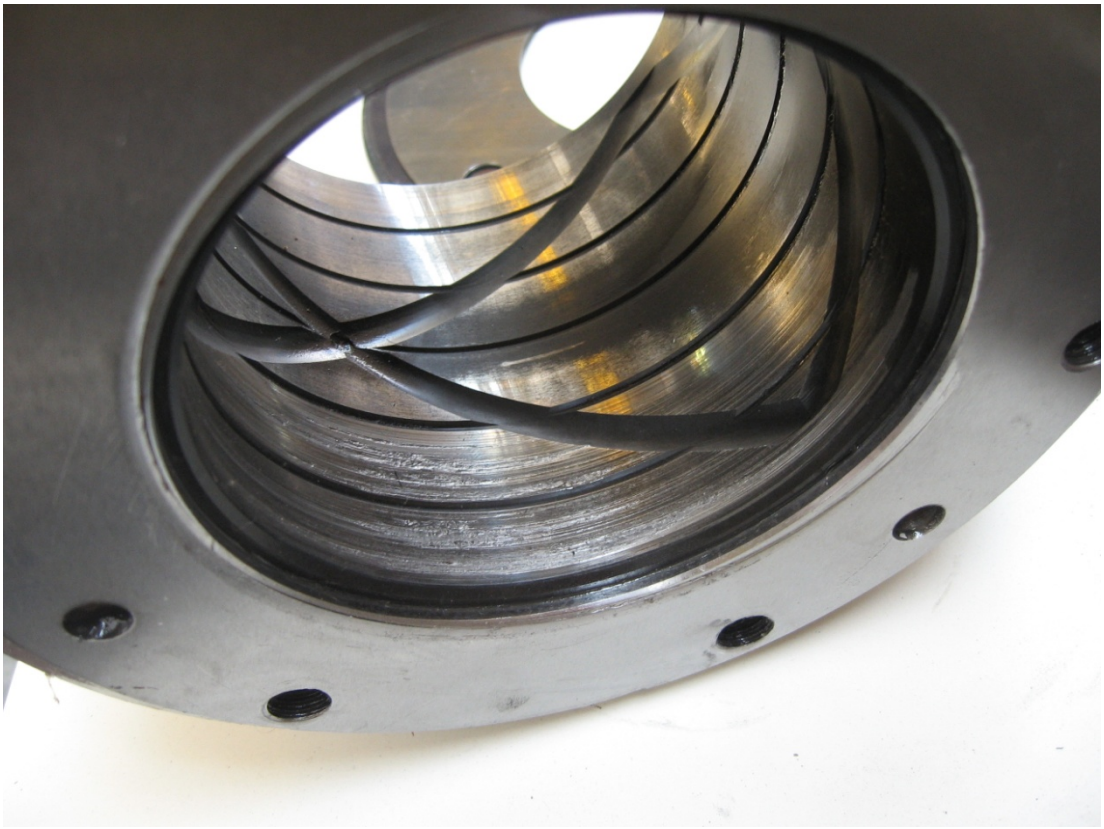

Figure 6.2 – Seizure region on the bearing for the 3rd test bearing

Seizure did not occur on the grooveless steel bearing, although it is tested under a PV value much higher than the ones in the tests of standard bearings. The force value of the sixth test is the same as the previous three tests, however, the bearing pressure decreased since the bearing area increased by 37% due to removing the grease grooves. That can be stated as an advantage of the grooveless bearing.

A local seizure is observed in the bronze bearing. The seizure did not either occur with a disturbing noise, or spread over the whole load bearing area. As can be seen from Figure 6.3, seizure only occurred on the portions where the pin does not contact any of the graphite plugs while in motion. When observing the surface from the center grease groove to the sides of the bearing, the seized surface rapidly changes into a smooth one, when the graphite layer is available on the surface. That shows the effect of lubrication on seizure.

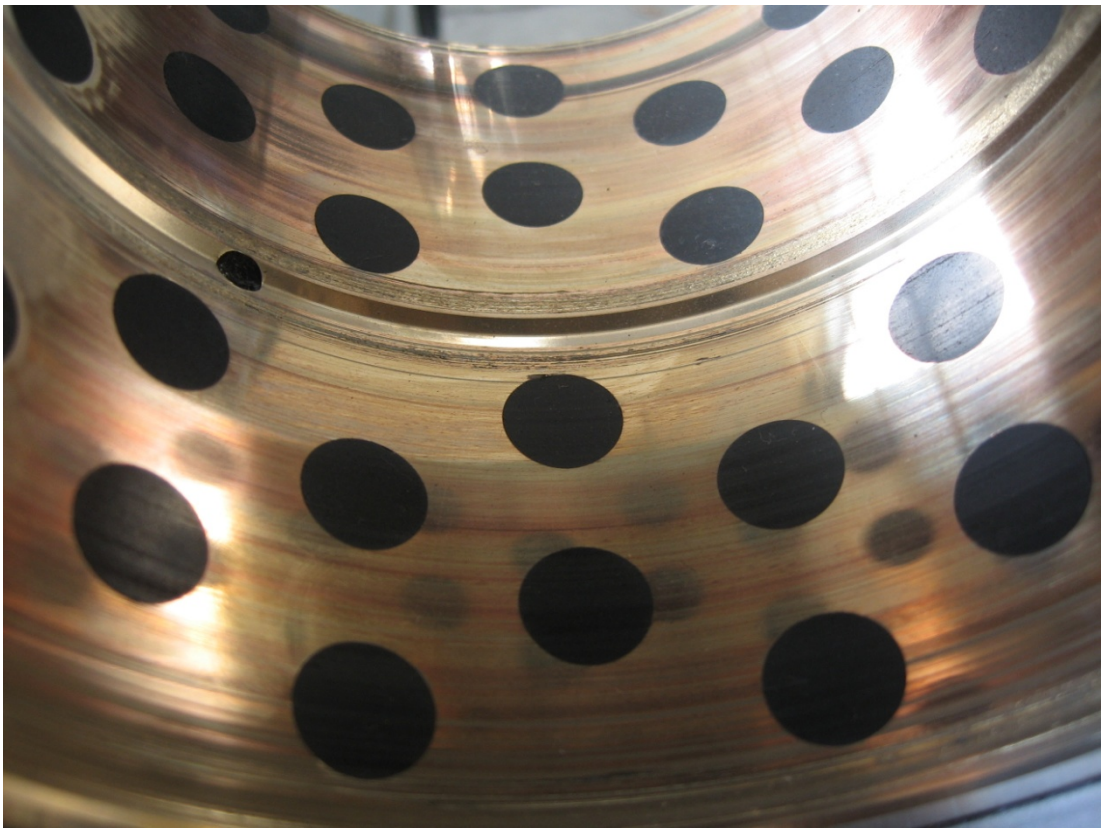

Figure 6.3 – The view of the bronze bearing after the test

The last test was performed to find out the life value of the bronze bearing under a predefined PV value. The load and velocity is limited by the maximum capacity of the test rig. A PV value of 0.47 MPa.m/s is applied to the bearing. No rapid breakdown or seizure occurred. Pit hole formation is observed on inner surface.

Figure 6.4 – Pit hole formation on the bronze test bearing

6.2.1. Bearing Inner Profile Measurements

The raw data of CMM measurements are the x, y and z coordinates of the scanned lines. It was seen that, the origin can not be placed at the same point and orientation in two scans, before and after the tests. Therefore, the data had to be manipulated. This manipulation was performed by coinciding the peak points of grooves or the line scan of the opposite side in the bearing. The groove profiles should coincide before and after the tests on these regions, since no wear is expected in the grooves or the opposite half of the bearing.

The test bearing inner circumference is measured from 2.5 mm below the bearing top surface. These measurements are performed for the steel bearings with grooves only; however, the scanned section does not contain any grooves. The profiles before and after the test are shown in Figure 6.5.

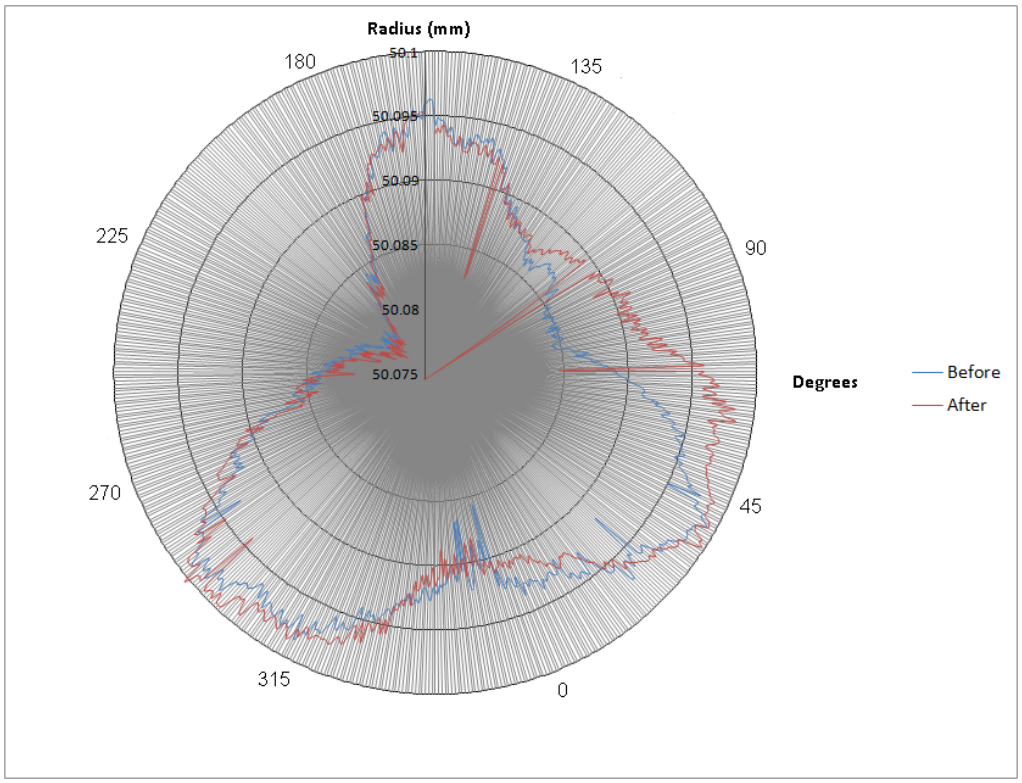

Figure 6.5 – Inner circumferential profile of the 2nd test bearing

As can be seen from Figure 6.5, there is approximately 20 microns of waviness profile on the circumference of the 2nd bearing. Other steel bearings with grooves bearings have this profile, as well. Equi-periodic behaviour of the wave strongly supports that it could have been caused by poor turning or grinding. This phenomenon may lead to uneven contact between pin and bearing. If grooves and these circumferential peaks coincide at the same point, highly localized contacts will occur, which may cause plastic deformation and debris formation. This may also explain the unstable seizure phenomenon on the standard steel bearings.

In second test, the bearing was loaded at 90°, and made an oscillation of ±45°. In the corresponding measurement, Figure 6.5, the oscillation motion is observed to give wear between 45° - 120°. The range is expected to be 35° - 145°, where 90° from the motion and 10° at both ends is caused by elastic deformation. The difference might occur either from the surface profile peak at 90°, or poor loading of test bench.

The radial wear profile changes along with the bearing. The behaviour can be observed in Figure 6.6 and Figure 6.7. Excluding z= -53.8 mm, all radii tend to increase from the maximum load angle (90°) to higher angle values. This contradicts the profile change of z = -2.5 mm in Figure 6.5. Therefore, it can be deduced that at different axial depth values, the waviness orientation, namely the angular position of peaks or valleys, differs; leading wear dominance on different sides of 90°.

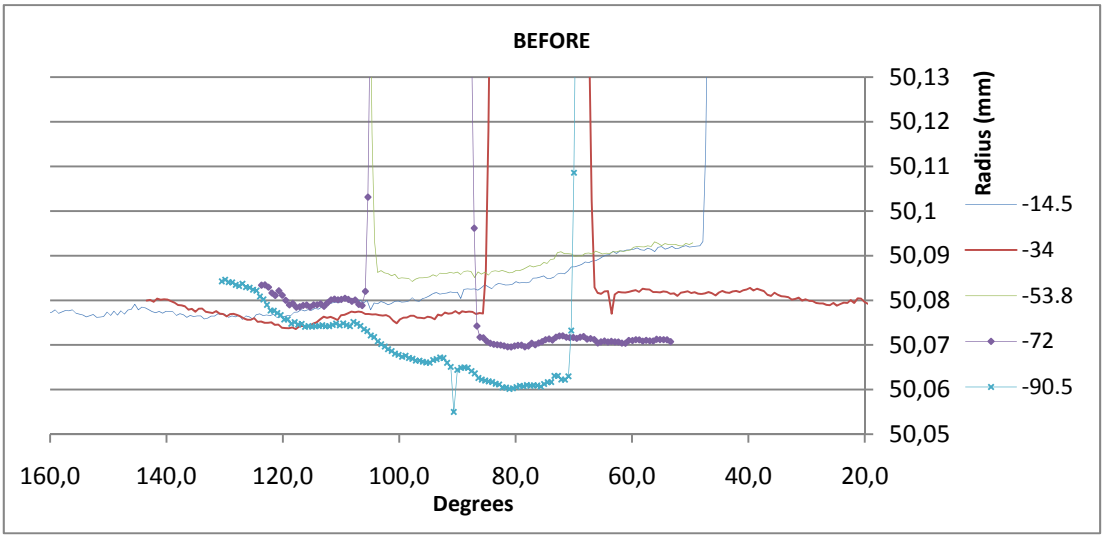

Figure 6.6 – Angular profiles of 2nd test bearing at several depths (Unworn)

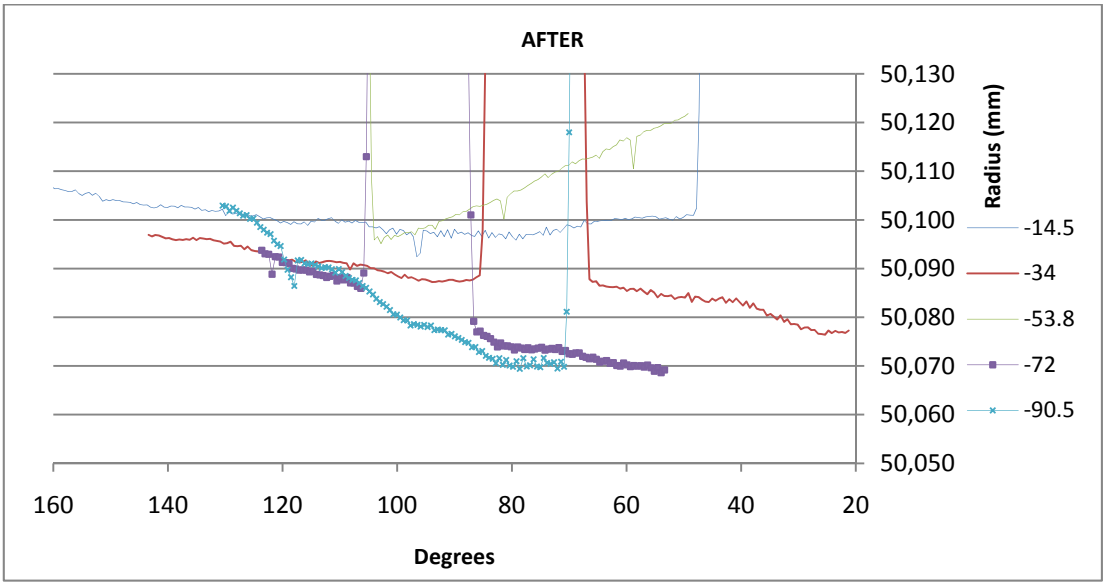

Figure 6.7 - Angular profiles of 2nd test bearing at several depths (Worn)

The data in Figure 6.8 show the surface profile of the second bearing in the axial direction, throughout the bearing width, 110 mm. Since the coordinate reference of CMM is not on bearing end, but on housing surface, the data starts from a negative value. Little or no wear is observed at the mid-section. This phenomenon, which was observed in all tests, is shown in Figure 6.9. The black-colored phosphate coating was removed from the sides but not from the middle of bearing width. The profile has an increasing trend both before and after the tests. This trend might either occur from an inclination of z-axis (along bearing axis) on the CMM while being created in the beginning of measurement, or an inclined position of bearing in its housing.

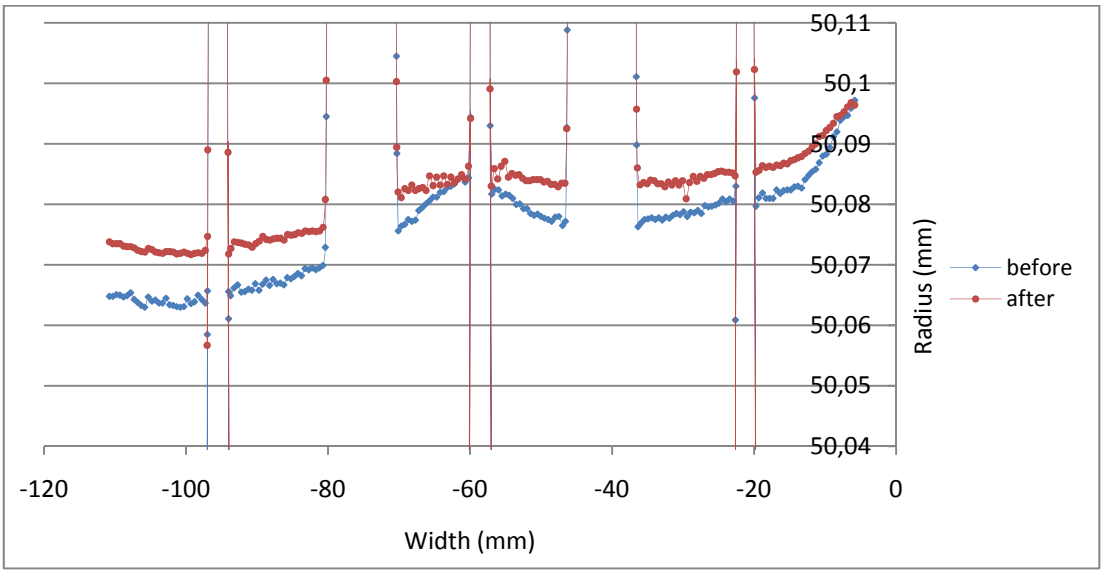

Figure 6.8 – The axial profile variations of the steel test bearing before and after the 2nd test

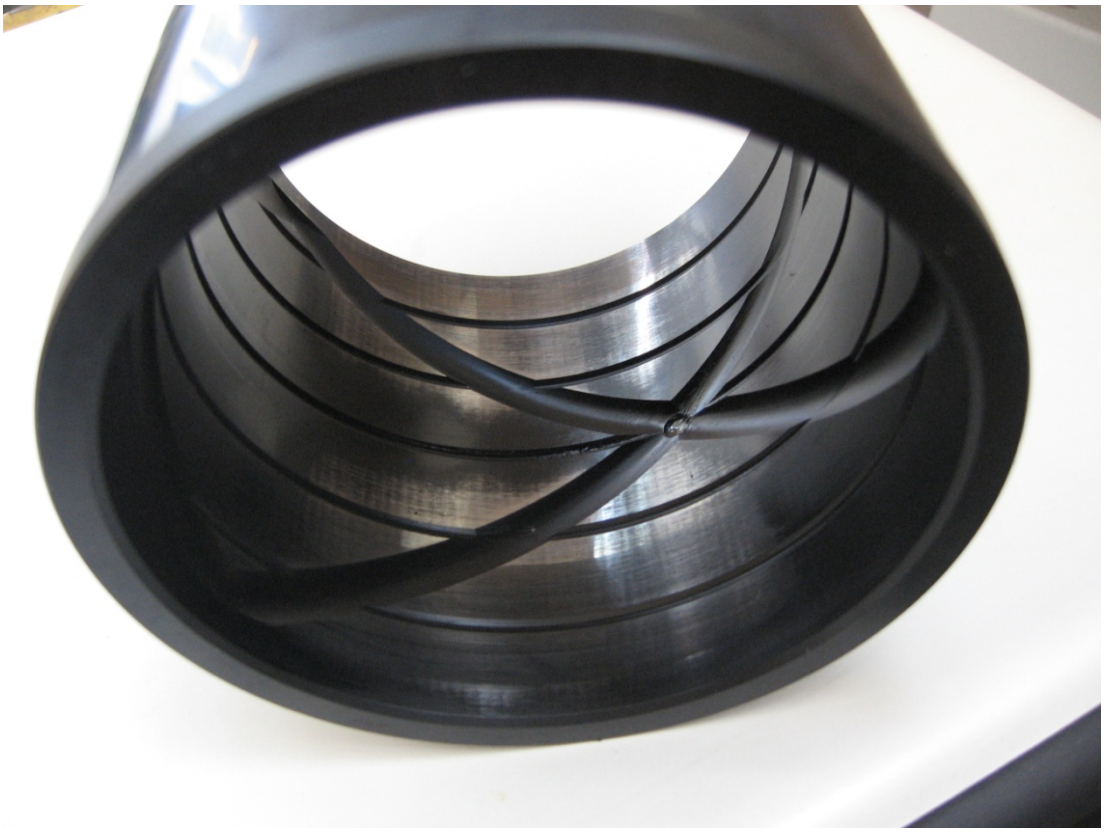

Figure 6.9 – A view of the 2nd test bearing

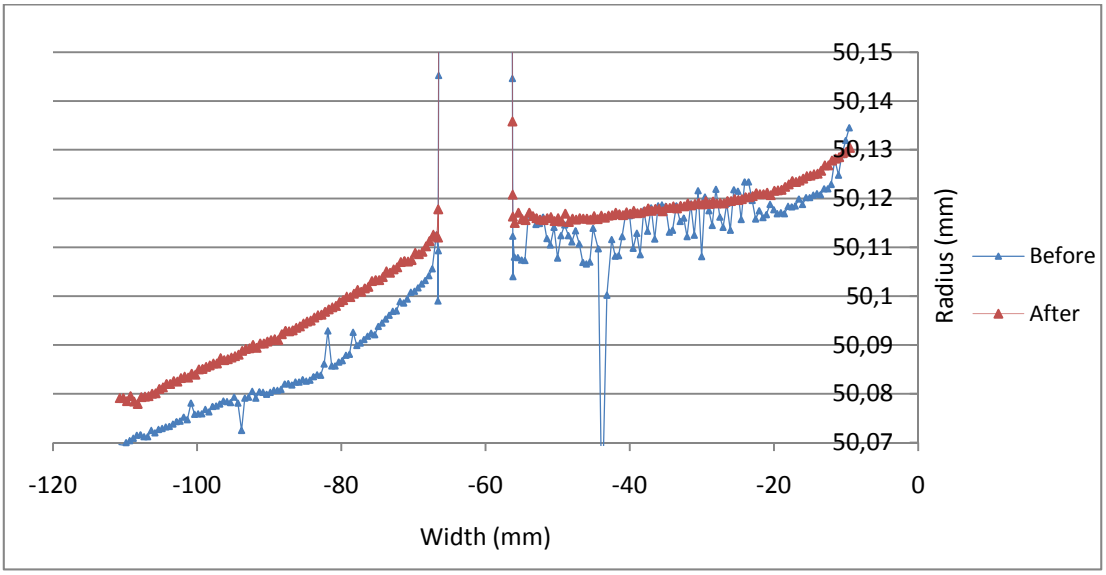

Figure 6.10 - The axial profile variations of the grooveless steel test bearing

Figure 6.10 shows the profile of the grooveless steel bearing in axial direction. Before the test, one half of the unworn bearing is observed to be much rougher than the other half. The fluctuations are in waviness scale. The reason for the phenomenon could not be understood. The fluctuations are in radial measurements, as well. However, this did not affect the wear volume calculation.

Figure 6.11 shows the profiles of the bronze bearing in axial direction before and after tests. The cyclic valleys of the "Before" data belongs to the graphite plugs. Since they protrude over the bronze surface, the radius value over them is smaller than that of bronze material. The wear is observed to change rapidly from 0.02 mm to 0.05 mm. The reason is the failure of the bolts on one side of the test housing. Therefore, the bearing might have been loaded more from the bolted side. This normally caused an unbalance of wear throughout the axial direction.

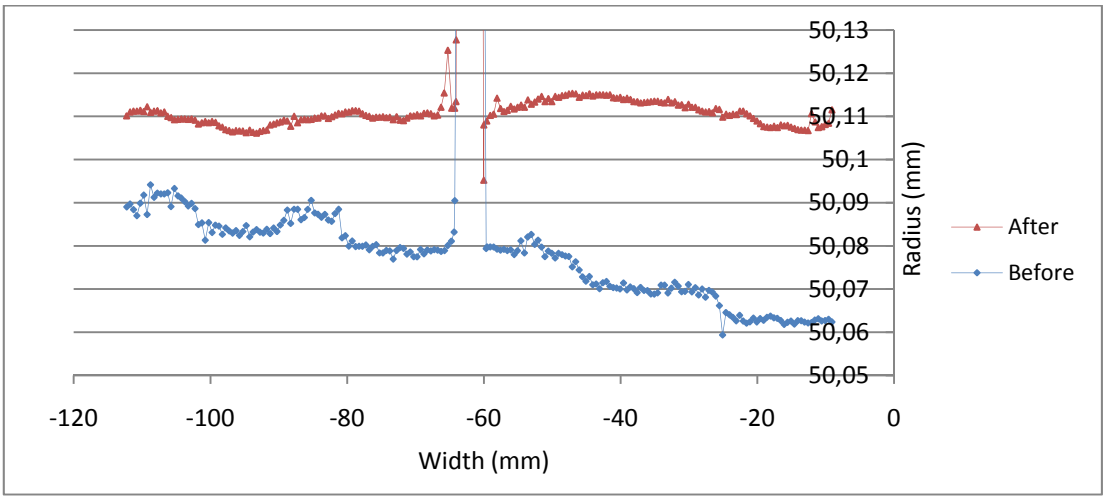

Figure 6.11 - The axial profile variations of the bronze test bearing

6.2.2. Total Wear and Wear Coefficient Calculation

The wear volume was calculated from the radial wear profiles. The radial surface profiles were measured at six different z values. The area between the profile before test and the profile after test gives the wear area of that particular cross-section. An example for the area determination for the bronze bearing is shown in Figure 6.12.

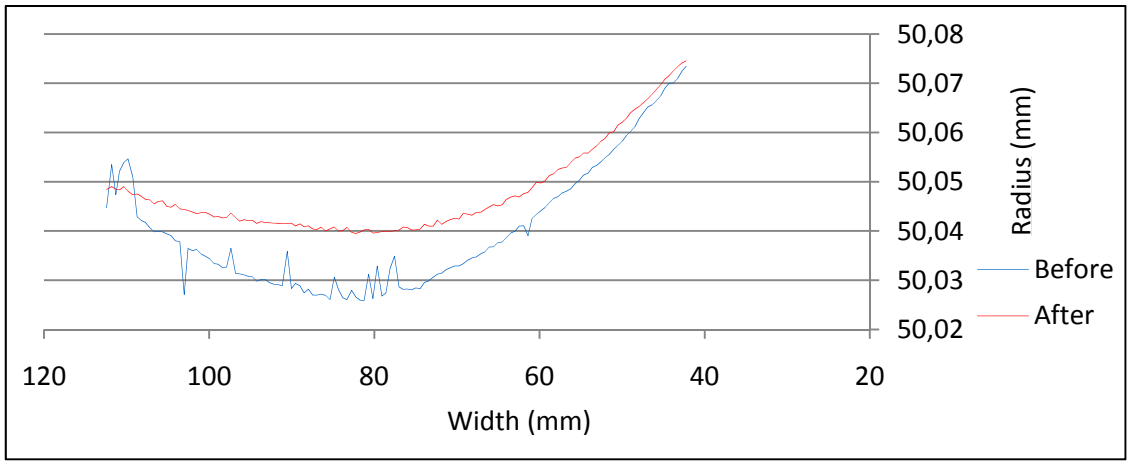

Figure 6.12 – Radial profiles of the bronze bearing before and after the tests for z=-89 mm

The wear area values for six different cross-sections were interpolated linearly throughout the bearing width and the points having the smallest and the largest z value are extrapolated to the ends of the bearing, as can be seen in Figure 6.13. Consequently, a wear volume was obtained for each bearing by calculating the areas under these curves.

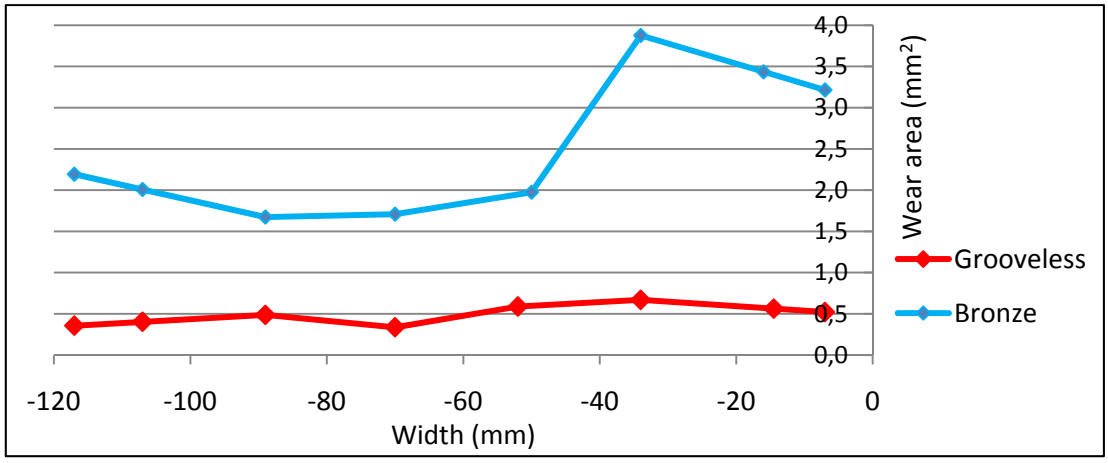

Figure 6.13 – Wear distribution throughout the bronze bearing axis

The radial profile measurement of the standard steel bearing was poor, which did not yield considerable wear values. This is observed in Figure 6.14.

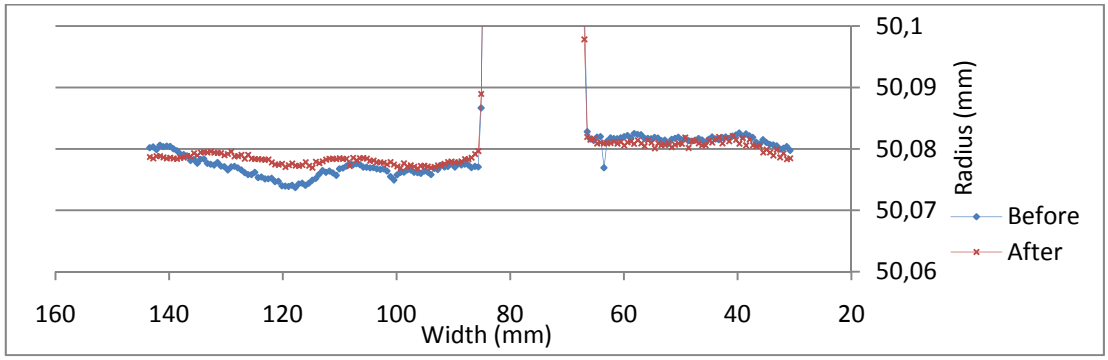

Figure 6.14 – Radial profiles of the 2nd test bearing before and after tests

Therefore, for the 2nd bearing wear volume calculation a different approach was used. From the radial measurements of the bronze bearing, one of which is given in Figure 6.12, a wear depth – wear area trend was formed. This trend, which comes out to be almost linear, is shown in Figure 6.15.

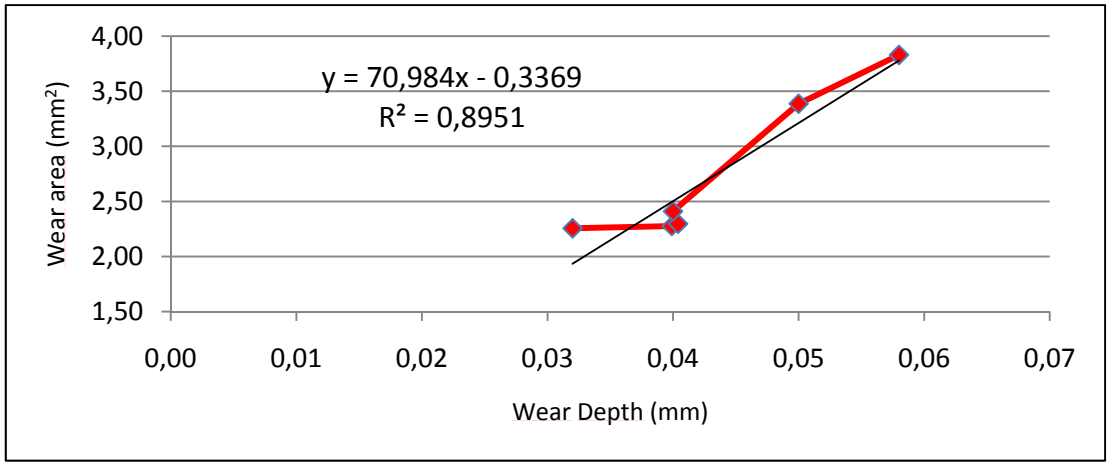

Figure 6.15 – Wear depth – wear area trend for the bronze bearing

Lastly, the resulting equation was integrated through the bearing width, using the wear depth plot, shown in Figure 6.8. This gives the wear volume for the 2nd bearing.

Wear coefficients are calculated by Archard's theory, using equation (3.1). Wear coefficients are given in Table 6-3.

Table 6-3 – Wear coefficient results of the tests

Test No:	**Bearing Type**	**PV (MPa.m/s)**	**Maximum Force (kN)**	**Sliding Distance (m)**	**Wear Volume (mm^3)**	**Wear Coefficient (mm^3/N.m)**
2	Standard steel	0.17	121	1418.1149	12.468	7.27E-08
6	Grooveless steel	0.41	200	2583.3316	55.39	1.07E-07
7	Bronze	0.41	200	2591.8139	265.6	5.12E-07

The wear coefficients of steel bearings were expected to be the same; however in the experimental study, the wear coefficients are observed to vary within 32% range. The reason for that variation is thought to be due to the measurement errors and the difference in wear area (volume) calculation methods from the experimental data.

6.2.3. Surface Roughness Measurements

The arithmetic average surface roughnesses (R_a) of test bearings are measured before and after the tests. The measurements are taken from unworn, worn and seized regions of the pins and bearings. The results are given in Table 6-4 and Table 6-5.

Table 6-4 – Surface roughness (R_a, μm) measured for the test bearings

	PV (MPa.m/s)	Cycle Time	Unworn	Worn	Seized
1. bearing	0.19	2007	0.46	0.25	2.27
2. bearing	0.12	9028	0.5	0.09	-
3. bearing	0.20	3710	0.73	0.53	4.2
Bronze bearing	0.41	16500	0.41	0.09	2.68

Table 6-5 - Surface roughness (R_a, μm) measured for the pins

	PV (MPa.m/s)	Cycle Time	Unworn	Worn	Seized
1. pin	0.19	2007	0.30	0.18	
2. pin	0.12	9028	0.37	0.13	-
3. pin	0.20	3710	0.40	0.04	3.46 - 7.42

As can be seen from the tables, continuous rubbing of surfaces decreases the surface roughness. This can also be observed by bare eye on the pin or bearing surfaces,

which become shiny, as if they are polished. Therefore, it can be said that real area of contact increases, as more cycles are completed.

When the dimensional change is observed in the axial profile graphs, the wear is observed to be in waviness level; beyond the level of surface roughness.

6.3. Conclusions

According to the pressure distribution calculation, no plastic deformation occurs on the pin or steel bearing. The seizure phenomenon is closely related to be lubrication quality. That is proven 1st, 3rd and 7th tests. Although the 3rd test had a higher PV value than the 1st one, it seized later than the 1st one; since it was lubricated more frequently. Again, in the 7th test only local seizure is observed where the pin does not contact graphite lubricant layer in operation.

All tests of standard steel bearings over PV=0.17 MPa.m/s value were ended with seizure. The reason might be the grooves for grease lubrication, because a test performed on the grooveless steel bearing at a higher PV value did not result in seizure, even for higher cycle times.

20 μm waviness is observed on the inner circumference of one of the steel bearings. This situation contributes to seizure or wear rate, because local contact occurs at different points. A more tight tolerance on waviness will bring longer life of bearings.

Life predictions can be made by using the wear coefficient values. Once, a maximum dimension change limit is determined, a life value can be calculated.

Since the steel bearing is harder than the bronze one, the wear volume for it also came out to be lower than that of the bronze bearing. Therefore, for both bearings,

not having any seizure phenomenon and having the least wear volume, the grooveless steel bearing is the best choice for usage.

6.4. Recommendations for Future Work

The tests performed so far should be repeated in order to form statistical data and tighter range of wear coefficient values. Besides, the wear volumes came out to be very low, which can lead to error easily. Therefore, following tests should last longer for consistent data.

The motor driving the motion line lets the user perform tests, which can sufficiently simulate the force and velocity values of the 22-ton excavator boom foot bearing. However, with the current electric motor, higher force or velocity values can not be achieved at the same time, since the electric motor starts drawing more current than its allowable value in those cases. The power of the electric motor driving the motion line can be increased to perform accelerated tests with higher force and velocity values.

Comparative tests including different parameters affecting wear can be performed in the future. Surface hardness, hardness variation in depth, and surface roughness are some of these parameters.

Hard sand particles can be problem especially in bucket bearings of the excavators. Therefore, the effect of hard particles trapped between mating surfaces can be observed with controlled introduction of hard particles. This can be satisfied by mixing the hard particles with grease and pumping it into the test bearing. Important point here is the homogeneity of the mixture.

REFERENCES

[1] *SAE Handbook – On Highway Vehicles and Off-Highway Machinery*, Society of Automative Engineers, 3, pp. 40.06, 1995

[2] Strand H., *Journal bearing housing design—A statistical study with FEM,* Tribology International, 40, pp. 665-671, 2007.

[3] ISO 4378-2: *Plain bearings – Terms, definitions, classifications and symbols – Friction and wear*.

[4] Shigley E., Mischke C., Budynas R., *Mechanical Engineering Design - International Edition,* McGraw-Hill, pp. 613, 2003

[5] Shell Retinax Grease EP2 Data Sheet

[6] Kim N. H.,Won D., Burris D., Holtkamp B., Gessel G. R., Swanson P., Sawyer W. G., *Finite element analysis and experiments of metal/metal wear in oscillatory contacts*, Wear 258, pp. 1787-1793, 2005.

[7] Dickrell D. J., Sawyer W. G., *Evolution of Wear in a Two-Dimensional Bushing*, Tribology Transactions, 47, pp. 257-262, 2004.

[8] Neale M. J., Gee M., *Guide to Wear Problems and Testing for Industry*, William Andrew Publishing, 2001

[9] Ukonsaari J., *Wear and friction of synthetic esters in a boundary lubricated journal bearing*, Tribology International, 36, pp. 821-826, 2003.

[10] Andersson P., Nikkila A, Lintula P., *Wear characteristics of water-lubricated SiC journal bearings in intermittent motion,* Wear, 179, pp. 57-62, 1994.

[11] Lu X., Khonsari M. M., *An Experimental Investigation of Dimple Effect on the Stribeck Curve of Journal Bearing,* Tribol Lett, 27, pp. 169–176, 2007.

[12] Tevrüz T., *Tribological behaviours of carbon filled polytetrafluoroethylene_PTFE / dry journal bearings*, Wear, 221, pp. 61-68, 1998.

[13] Tamura K., Ishihara S., Goshima T., Tachi Y., *Effect of cyclic load and sliding speed on the sliding wear characteristics of a bearing lined with WJ7 white metal,* Proc. Instn Mech. Engrs Part J: J. Engineering Tribology, 218, pp. 23-31, 2004.

[14] Bierlein J. C., Lisowsky B., Killian M. L., Ahmad A., *Sliding Contact Test for Engineered Surfaces,* Tribology Transactions, 47, pp. 549-556, 2004.

[15] Zhang C., Cheng H. S., Wang Q. J., *Scuffing Behaviour of Piston-Pin/Bore Bearing in Mixed Lubrication- Part 2: Scuffing Mechanism and Failure Criterion,* Tribology Transactions, 47, pp. 149-156, 2004.

[16] Hiraoka N., *Wear life mechanism of journal bearings with bonded MoS_2 film lubricants in air and vacuum,* Wear, 249, pp. 1014 – 1020, 2002.

[17] ISO 7148-1: *Plain bearings – Testing of the tribological behaviour of bearing materials.- Part 1: Testing of bearing metals.*

[18] Marklud P., Larsson R., *Wet clutch friction characteristics obtained from simplified pin on disc test,* Tribology International, 41, pp. 824-830, 2008.

[19] Koszela W., Galda L., Dzierwa A., Pawlus P., *The effect of surface texturing on seizure resistance of a steel–bronze assembly,* Tribology International, 43, pp. 1933-1942, 2010.

[20] Siu J. H. W., Li L. K. Y., *An investigation of the effect of surface roughness and coating thickness on the friction and wear behaviour of a commercial MoS_2 –metal coating on AISI 400C steel*, Wear, 237, pp. 283 – 287, 2000.

[21] Stachowiak G. W., Batchelor A. W., *Engineering tribology,* Butterworth-Heinemann, 2nd edition, 2001.

[22] Ciavarella M., Decuzzi P., *The state of stress induced by the plane frictionless cylindrical contact. I. The case of elastic similarity,* International Journal of Solids and Structures, 38, pp. 4507 – 4523, 2001.

APPENDIX A

ENGINEERING DRAWINGS OF THE TEXT COMPONENTS

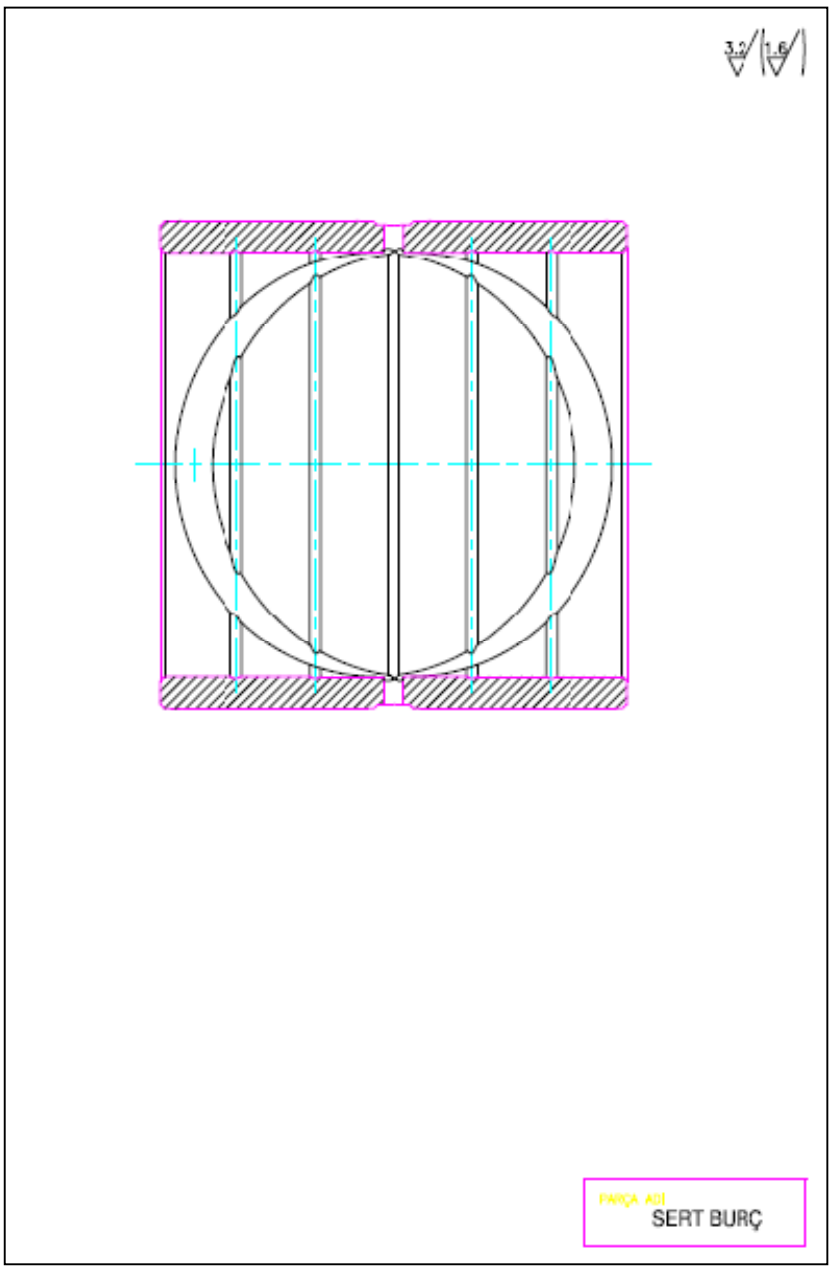

Figure A.1 - The engineering drawing of the steel test bearing

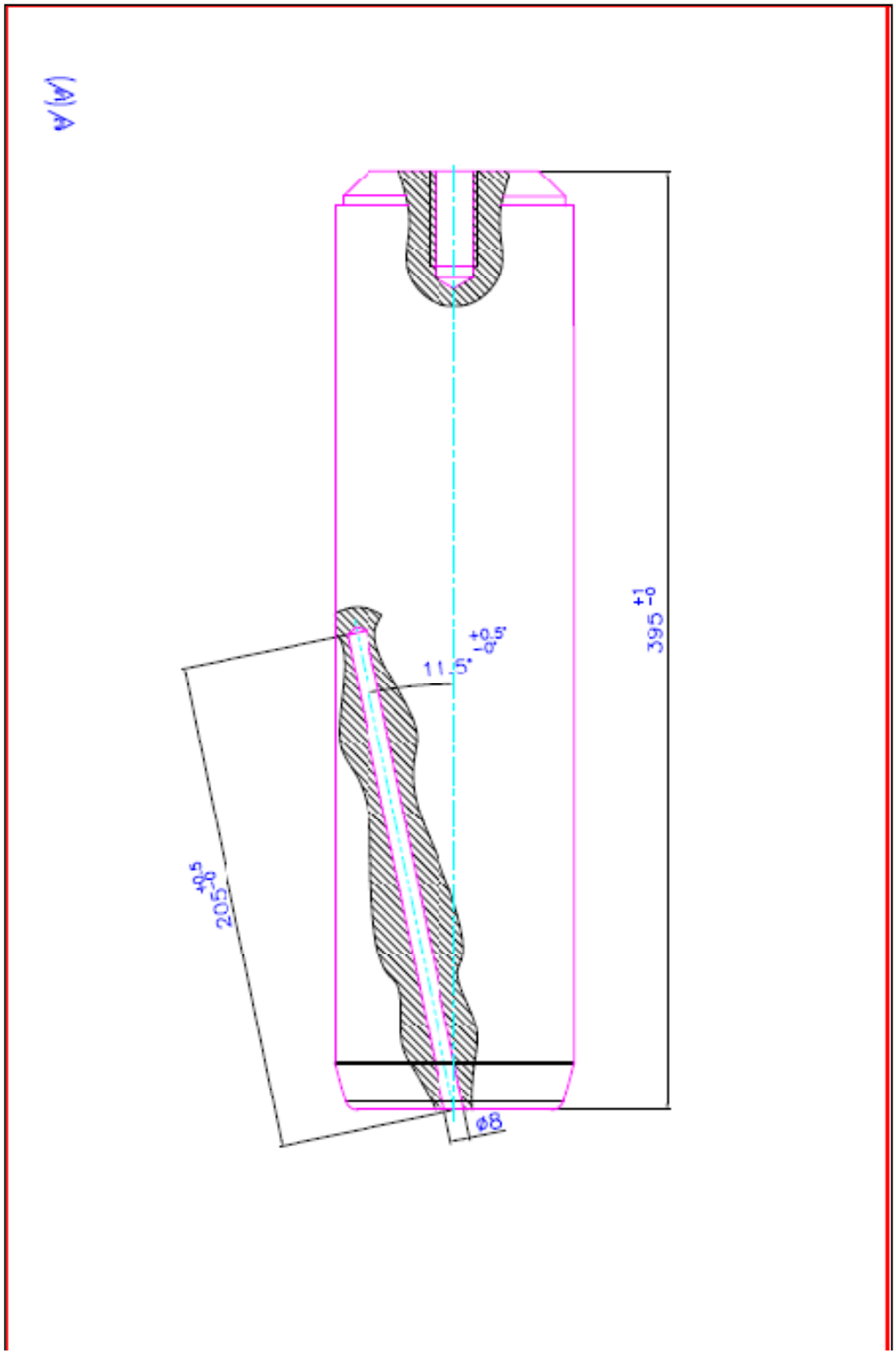

Figure A.2 – The engineering drawing of the test pin

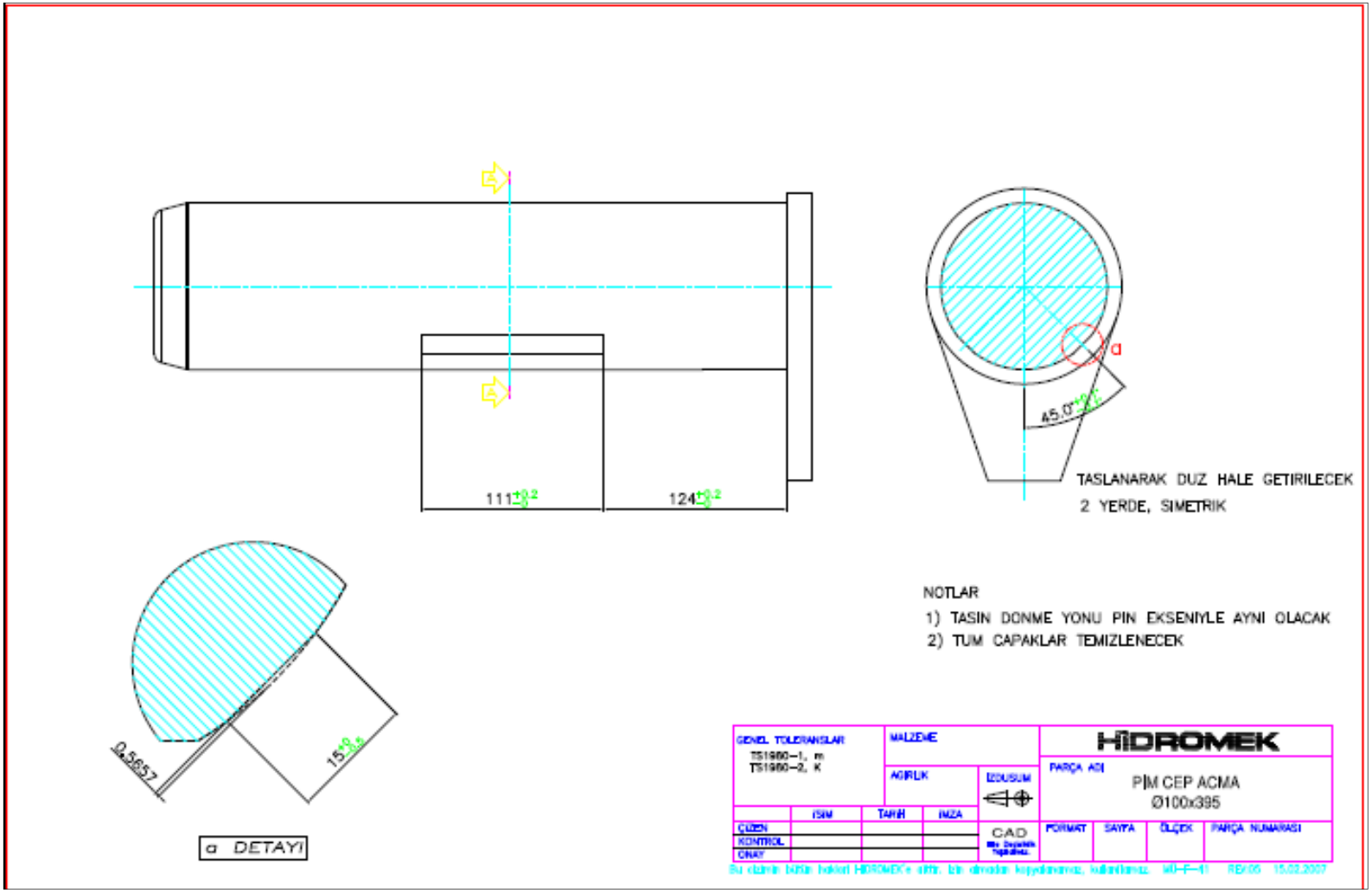

Figure A.3 – The engineering drawing of the channels on the modified pin

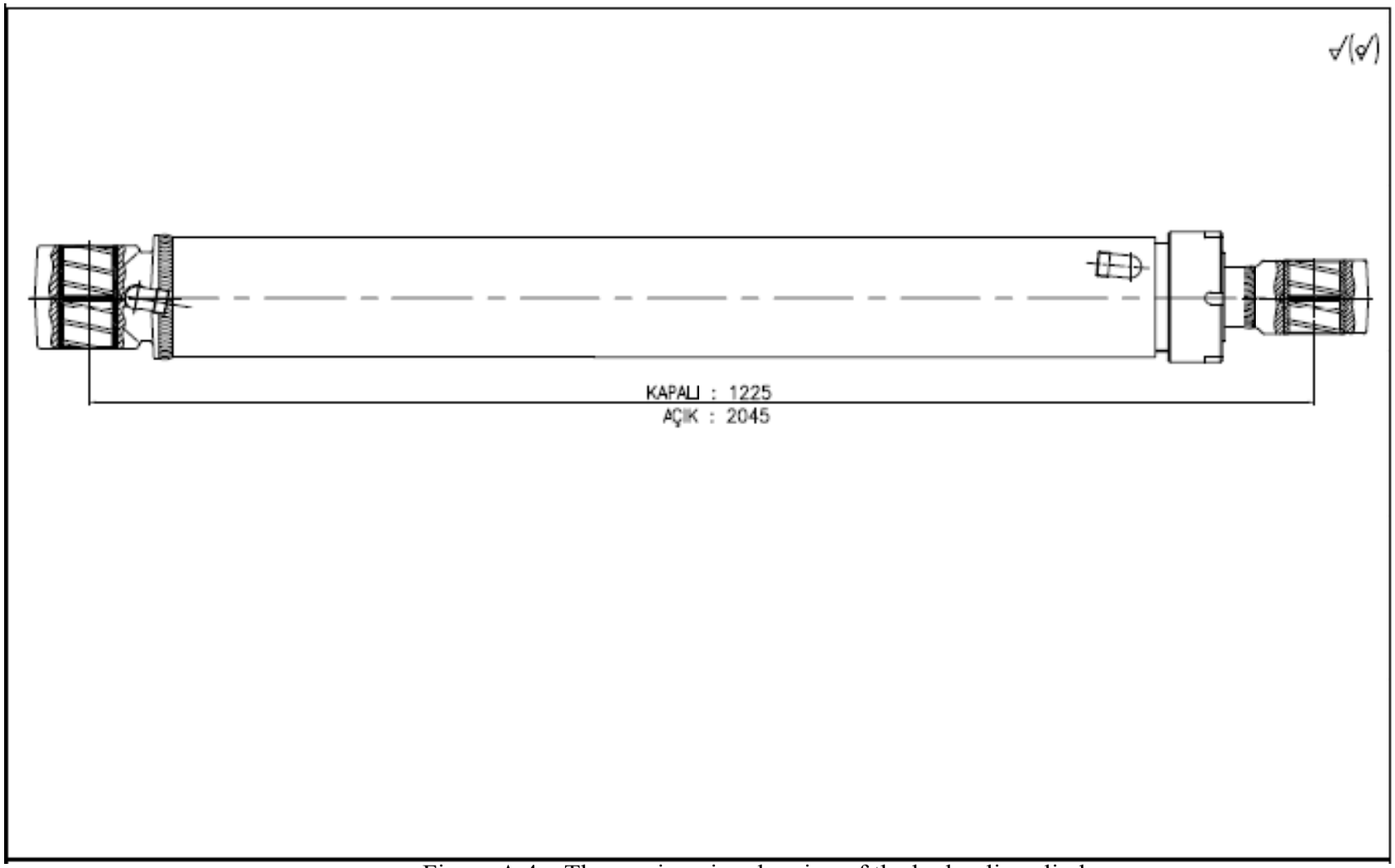

Figure A.4 – The engineering drawing of the hydraulic cylinder

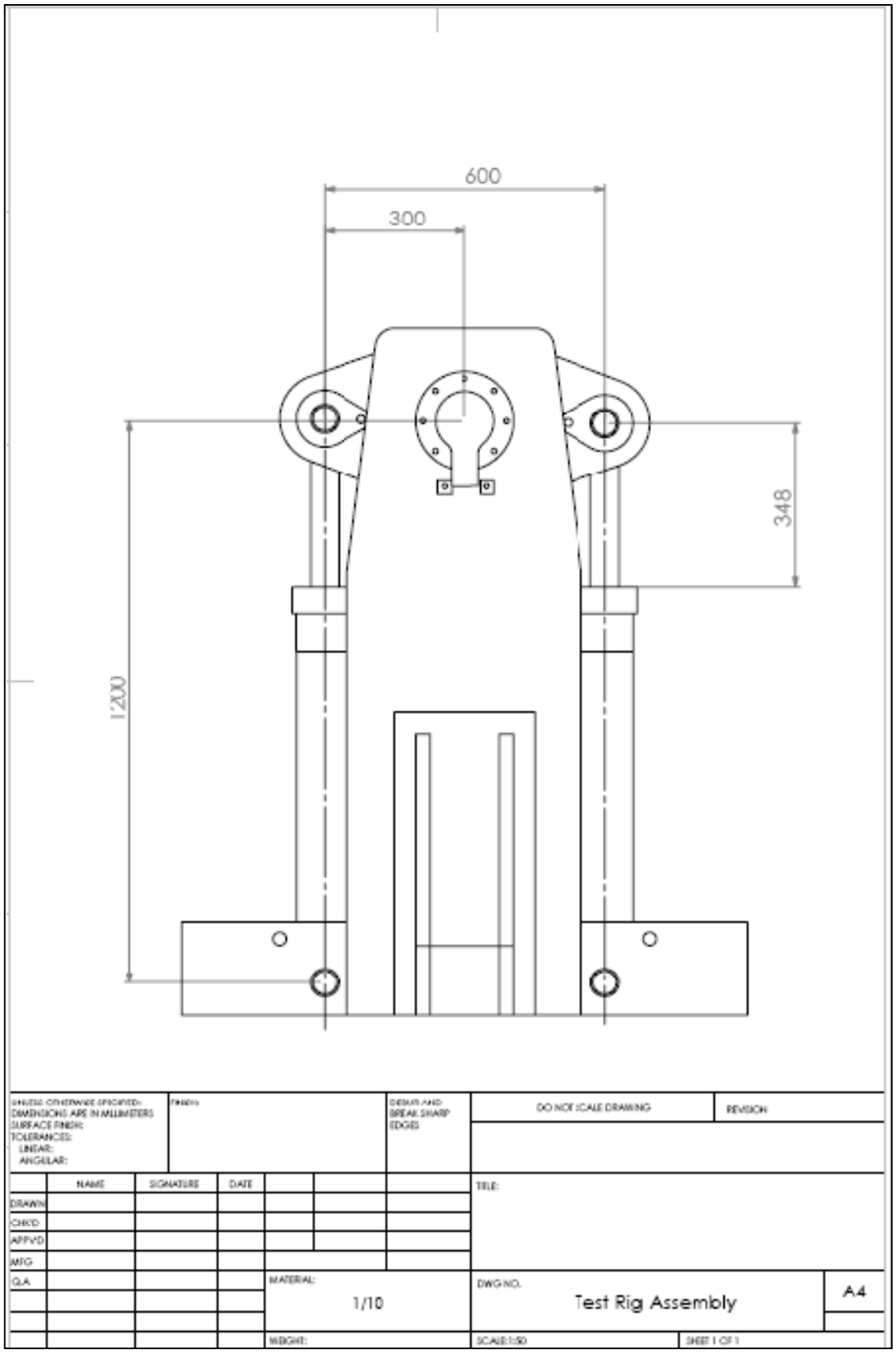

Figure A.5 – The engineering drawing of the bench assembly

APPENDIX B

CALCULATION OF TOTAL FORCE USING THE HYDRAULIC PRESSURES

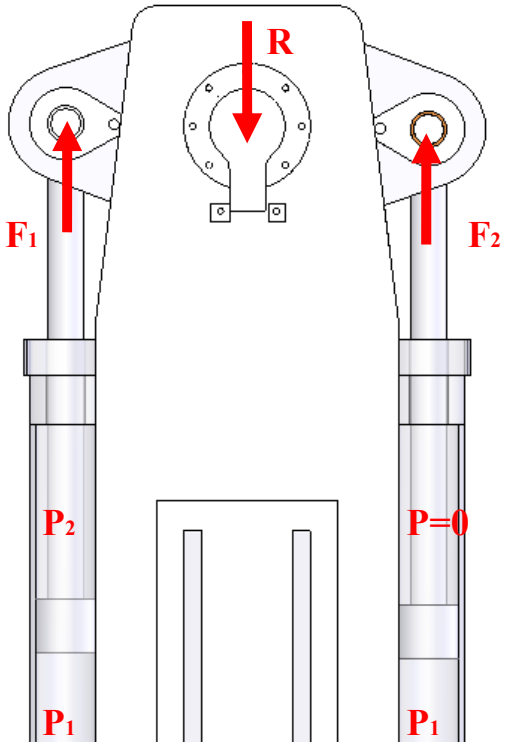

Figure B.1 – Hydraulic cylinder pressures and total force on the test pin

The total force, R, on the test bearing is determined by the hydraulic system pressure. Two hydraulic cylinders having pipe and rod diameters 100 mm and 60 mm, respectively are used. The top sides (Φ100) are pressurized to P_1, the main pressure. While there is motion the rod side (Φ60) of one of the cylinders is pressurized to P_2 value, which also determines the closing velocity of the hydraulic cylinder. The other

rod side opens to the tank; therefore the pressure is zero here. When the arm oscillates to the other side, P_2 and zero pressure switches each other, but total force on the pin is the same.

The total force on the test pin can be calculated as follows.

$$F = F_1 + F_2 \tag{B.1}$$

$$F1 = P_1 \text{ x } A_1 - P_2 \text{ x } A_2 \tag{B.2}$$

$$F2 = P_1 \text{ x } A_1 \tag{B.3}$$

$$F = 2 \text{ x } P_1 \text{ x } A_1 - P_2 \text{ x } A_2 \tag{B.4}$$

Where A_1 is the area of top side, A_2 is the area of rod side of the hydraulic cylinder. Using the diameter values:

$$A_1 = \frac{100^2 \text{ x } \pi}{4} \tag{B.5}$$

$$A_1 = 7853 \text{ mm}^2 \tag{B.6}$$

$$A_1 = \frac{(100^2 - 60^2) \text{ x } \pi}{4} \tag{B.7}$$

$$A_1 = 5026 \text{ mm}^2 \tag{B.8}$$

$$F = 15706 \text{ x } P_1 - 5026 \text{ x } P_2 \tag{B.9}$$

APPENDIX C

CALCULATION OF PV VALUE FOR OSCILLATING BEARINGS

The average bearing pressure is based upon the projected area of bearing. It is given by the equation (1.5). The sliding velocity is calculated by dividing the total sliding distance by time [2].

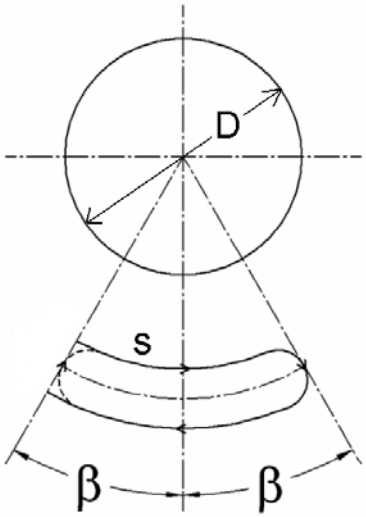

Figure C.1 – Oscillating motion definition [2]

The sliding distance in one cycle can be calculated by:

$$s = \frac{4\beta}{360}\frac{\pi D}{1000} \tag{C.1}$$

Where β is the oscillation angle in degrees and D is the diameter of the bearing. Sliding distance, s, here is in meters.

Hence, the velocity can be calculated by the equation (C.2). N_{osc} is the number of cycles per minute and in meters per second.

$$V = \frac{4\beta\pi D N_{osc}}{360 \text{ x } 1000 \text{ x } 60} \tag{C.2}$$

PV can be found by multiplying (1.5) and (C.2). The unit is MPa.m/s.

$$PV = \frac{F}{D \text{ x } w} \frac{4\beta\pi D N_{osc}}{360 \text{ x } 1000 \text{ x } 60} \tag{C.3}$$